RSC Advances

ROYAL SOCIETY OF CHEMISTRY

www.rsc.org/advances

Asphaltene: Structural Characterization, Molecular Functionalization, and Application as Low-cost Filler in Epoxy Composites

Hongchao Wu[1], *Michael R. Kessler*[1,2,3*]

[1]Department of Materials Science and Engineering, Iowa State University, Ames, IA

[2]Ames Laboratory, US Department of Energy, Ames, IA

[3]School of Mechanical and Materials Engineering, Washington State University, Pullman, WA

Abstract

Asphaltene obtained by extraction from asphalt was investigated by different analytical techniques in order to characterize its composition, molecular structure and morphology. Then, the asphaltene molecules were successfully functionalized by 3-glycidyloxypropyltrimethoxysilane and 3-aminopropyltriethoxysilane as confirmed by thermogravimetric analysis, X-ray photoelectron spectroscopy, and Fourier transforms infrared spectroscopy. Finally, asphaltene/epoxy composites at four different loading levels were prepared and their thermo-mechanical properties were examined. The thermal analysis results indicated that asphaltene as novel reinforcing filler in epoxy resin caused a significant increase in storage modulus of both glassy and rubbery regions, slightly increased the glass transition temperature without negatively affecting thermal stability, and reduced the overall cost of the material.

1. Introduction

Asphaltenes is the heaviest and complicated hydrocarbons component in crude oil along with paraffins, resins, aromatics and napthenes[1]. It can be general identified as polynuclear aromatics

*Corresponding author: MichaelR.Kessler@wsu.edu

with significant molecular mass, aromaticity, and heteroatom contents. It is well understood that flocculation and self-aggregation of asphaltene molecules may result in the formation of coke-like precursors that are responsible for plugging well bores and flow lines, blocking transfer pipelines[2], and deactivating catalytic reactions during upgrading and refining processes[3]. A variety of molecular interactions contributing to the aggregation of asphaltene molecules and to the formation of colloidal particles in crude oil include hydrogen bond forces, aromatic π-π* stacking forces[4-5], polarity induction forces[6], and electrostatic attractions between the molecules[7-8]. Although this certainly part of the effort, more attention has been paid to learn about the factors that influence the stability of asphaltenes – which has as much to do with its composition and molecular structure as with the crude oil in which it is contained. A complete molecular analysis of asphaltene has not yet been achieved because of its strong tendency to agglomerate and the variation in molecular structures depended on the its origin, but it is generally acknowledged that asphaltene molecules consist of fused poly-condensed aromatic and naphtenic unit cores that surrounded by alicyclic and aliphatic side chain substituents with heteroatoms such as nitrogen, sulfur, and oxygen, and traces of metal elements[9].

Epoxy matrix composites have attracted a wide range of research interest in recent years because of their potential applications in various fields, such as in aerospace engineering and in the automotive and packaging industries. In recent decades, the incorporation of various kinds of fillers into epoxies was investigated to improve specific properties. For instance, nanoclay fillers in epoxy resin were studied to improve mechanical properties[10-11]; dielectric properties of epoxy composites were enhanced by the introduction of $BaTiO_3$ particles into the matrix[12]; thermal conductivity of epoxy resin was increased by reinforcement with boron nitride nanoplatelets[13]; and the thermal expansion behavior of epoxy resin was tailored by adding ZrW_2O_8

nanoparticles[14]. However, high cost for both materials and processing techniques still restrain the industrial scale-up of epoxy matrix composites and motivate investigations of low-cost fillers for composite applications.

Asphaltene, which is obtained from the abundant by-product of the petroleum industry, is reported as a potential source of pure carbon microspheres[15] and fibers[16]. Asphaltene also provides stiffness and mechanical strength to bitumen by holding the overall structure[17]. Its rigid molecular characteristic makes asphaltene a potential candidate as value-added, reinforcing filler in polymer composites. Due to the surface chemistry of filler is critical for the performance of polymer composites, appropriate surface treatments, such as coupling agents[18-20], surfactants[21-22], and functionalized polymers[23], were studied to facilitate enhanced compatibility and strong interfacial bonding between filler and polymer matrix. In this work, asphaltene is extracted from asphalt and undergoes further molecular modification through two different silane-coupling agents to facilitate the preparation of low-cost asphaltene/epoxy resin composites.

2. Experimental Section

2.1. Materials

The asphalt used as the raw material for the isolation of asphaltene was identified as AAB-1 according to the Strategic Highway Research Program's Materials Reference Library (MRL). *n*-heptane, toluene (reagent), and HPLC tetrahydrofuran (THF) were purchased from Fisher Scientific and used as received. Two silane coupling agents, 3-glycidyloxypropyltrimethoxysilane 99% (GPTMS) and 3-aminopropyltriethoxysilane 98% (APTES) were obtained from Sigma-Aldrich. Bisphenol A diglycidyl ether (with the trade name of EPON 828) was purchased from Hexion Specialty Chemicals, Inc. The curing agent (Versamid 140) was purchased from Cognis/BASF.

2.2. **Extraction of asphaltene**

Asphaltene was separated from the asphalt using a SARA (saturates-aromatics-resins-asphaltenes) fractionation strategy reported by S. Chiaberge *et al.*[9]. Firstly, hot toluene was gently stirred with asphalt (volume/mass ratio = 5:1) for 1 h at 60 °C. The solution was then filtered through a 0.45 μm filter membrane to separate the filtrate and undissolved components. Afterward, toluene was removed using a rotary vaporator and the toluene-free asphalt was further mixed with *n*-heptane at a volume/mass ratio of 40:1 to precipitate the asphaltene. The mixture was stirred for 4 h at 80 °C and left in a dark cabinet overnight for full precipitation. Subsequently, the mixture was filtered with a 0.45 μm filter membrane to collect the non-filterable substances (asphaltene). To fully remove the waxy substances, the filtered material was further washed using boiled *n*-heptane in a Soxhlet apparatus for 24 h until the filtrate solution became colorless. The acquired dark-brown solid asphaltene was finally dried in a vacuum oven at 70 °C overnight to evaporate any residual solvent.

2.3. **Molecular modification of asphaltene**

In order to perform the molecular functionalization, 0.5 g of prepared pristine asphaltene powder was dissolved in 100 ml tetrahydrofuran (THF) as the reaction medium and 1 ml of APTES or GPTMS were added under stirring at 65 °C for 24 h. After evaporation of THF, the obtained silane-treated asphaltene was further washed with excess ethanol to remove the unreacted silanes and then placed in a vacuum oven at 80 °C overnight to eliminate solvent residue in the samples.

2.4. **Preparation of asphaltene/epoxy composites**

The asphaltene/epoxy composites were prepared *via* the following route: Firstly, asphaltene was fully dissolved in THF at a concentration of 0.5 g/ml, followed by mixing with a calculated amount of epoxy pre-polymer in THF solvent for 4 h at 70 °C to facilitate molecular interaction

between filler and matrix through aromatic π-π* stacking and the formation of chemical bonds between functional groups. After evaporation of THF from the mixture in a vacuum oven, the curing agent (Versamid 140) was introduced and mixed with the suspension containing epoxy pre-polymer and asphaltene at a high shearing rate in a planetary mixer. Subsequently, the slurry was poured into a silicone rubber mold (20 mm × 20 mm × 3.5 mm) and degassed for 30 min in a vacuum oven. Finally, the black, homogeneous, and bubble-free composites were moved to a convection oven and cured at 75 °C for 16 h followed by post-curing at 140 °C for 2 h.

2.5. **Measurement and characterization**

Elemental analysis was performed on a Perkin Elmer 2100 Series II CHN/S analyzer. Each asphaltene sample was run four times to determine an average value of the weight percent for different elements. Fourier Transform Infrared Spectroscopy (FTIR) was carried out on an IRAffinity-1 Fourier Transform Infrared Spectrophotometer from Shimadzu. The asphaltene powder was finely ground with KBr powder and pressed into circular pellets for measurement. All the absorption spectra were acquired from 500 to 4000 cm^{-1} with 48 scans and a resolution of 4 cm^{-1}, and a baseline-correction was performed prior to the analysis. Raman spectra were recorded at room temperature in a range from 1000 to 2000 cm^{-1} on a Renishaw Dispersive Raman Spectrometer with a 480 nm solid-state laser as the excitation source. A small amount of asphaltene powder was finely mortared and then deposited onto a microscope glass slide, followed by manually pressing to smooth the sample prior to the measurement. X-ray photoelectron spectroscopy (XPS) analysis was conducted on a PHI55000 XPS with an Al Kα source (1486.6 eV). Specifically, the survey spectra were collected from 0 to 1100 eV with a pass energy of 187.85 eV and a step size of 0.8 eV; high-resolution spectra for specific elements were acquired with a pass energy of 58.70 eV and a step size of 0.25 eV. The morphology of the

asphaltene powder was characterized using a FEI Quanta 250 field emission scanning electron microscope (SEM) at 10.00 kV under high vacuum. A small amount of asphaltene powder was ultrasonicated in acetone for 2-3 h prior to SEM measurements. A Q50 thermogravimetric analyzer (TGA) from TA Instruments was employed to study the thermal degradation behavior of untreated and functionalized asphaltene, and to determine the thermal stability of asphaltene/epoxy composites from room temperature to 800 °C at a heating rate of 20 °C/min in air and nitrogen atmospheres, respectively. Dynamic mechanical properties of the asphaltene/epoxy composites were measured using a Q800 dynamic mechanical analyzer (DMA) from TA Instruments. Four specimens with dimensions of 6 mm × 3 mm × 1 mm were cut and tested in three-point bending mode at an amplitude of 10 μm and a frequency of 1 Hz. Data were acquired from –20 to 200 °C at a rate of 5 °C/min.

3. Results and discussion

3.1. Characterization of pristine asphaltene

Table 1 shows the result of the elemental analysis, which provides the weight percentages of C, H, N, S, and O in pristine asphaltene. The data shows that carbon was the major element of composition in asphaltene together with smaller amounts of hydrogen and other heteroatoms (N, S, and O). In addition, the ratio of H to C (~1.1) indicated highly aromaticity of the asphaltene molecules[24]. The relative total heteroatoms/carbon ratio [(N+S+O)/C] was similar to that found in a previous study[25].

The obtained FTIR absorption spectrum of extracted asphaltene is shown in Figure 1, which exhibited similar characteristic peaks as seen in previous studies[9, 25-26]. Based on its complicated molecular structure, the featured peaks could be categorized into three sections: aromaticity, aliphaticity, and polar functionality[25]. Specifically, for the aromatic moiety, the detected

adsorption bands at 750, 808, and 866 cm^{-1} corresponded to the out-of-plane C-H bending in 1,2-disubstituted aromatic, 1,4-substituted aromatic, and 1,3-disubstituted aromatic, respectively; C=C stretching vibration in the aromatic structure was assigned at 1602 cm^{-1}. For the aliphatic characteristic, C-H stretching vibrations of CH_2 and CH_3 were assigned at 2922 and 2852 cm^{-1}, while the peaks at 1458 and 1375 cm^{-1} represented the C-H bending vibration of CH_2 and CH_3. For polar functionalities, stretching vibrations of –OH and/or –NH appeared at around 3458 cm^{-1}; and stretching vibrations of S=O in sulfoxides was observed at 1031 cm^{-1}.

Raman spectroscopy was used to study the molecular bond vibrations caused by intra- and intermolecular interactions of asphaltene[27]. Figure 2 shows that the Raman spectra of asphaltene exhibited two distinct bands at around 1580 cm^{-1} and 1350 cm^{-1}, which corresponded to G and D1 bands, respectively[28]. The sharper G peak in comparison to the broader D1 peak indicated the existence of a short-range order of the aromatic sheet of asphaltene[27-28]. In this study, the summation of four peaks (1350, 1500, 1580, and 1620 cm^{-1}) was used to fit the Lorentzian function with Origin 9 software following previous research[28]; it proved to be an excellent match for the experimental spectra as exhibited in Figure 2. Most importantly, the size of the aromatic core structure (L_a) could be determined based on Equation (1) proposed by Tuinstra and Koenig[29]:

$$L_a = 4.4\frac{I_G}{I_{D1}} \quad (1)$$

where, I_G and I_{D1} are the integrated peak intensities of the G and D1 bands after curve fitting. To obtain statistically relevant data and to examine the reproducibility of the measurement, spectra were collected from five random locations on the flat surface of each prepared sample. Table 2 lists the deconvolution data and the calculated value for L_a of the asphaltenes determined at the

chosen locations. It was found that the actual peak positions were at approx. 1349, 1497, 1569 and 1601 cm^{-1}. In addition, the value of L_a was calculated as 1.74 nm, which suggested that approx. 6 to 7 aromatic rings were fused together during the formation of the poly-aromatic core of the asphaltene molecules.

The result of XPS measurements suggested that asphaltene is comprised primarily of carbon atoms (94.16%) and a minor amount of heteroatoms (2.40% oxygen, 1.51% nitrogen, and 1.90% sulfur) as shown in Table 3, which is in good agreement with the result from elemental analysis. The binding types of each atom in asphaltene were investigated by curve-fitting of individual high-resolution XPS spectra. Figure 3 displays the high-resolution spectra for different atoms along with their fittings by deconvolution performed with CasaXPS software using a Gaussian-Lorentzian hybrid function. Regarding the C 1s peak, three peaks were chosen for fitting at approx. 284 eV, 287 eV, and 289 eV, which are attributed to carbon in aliphatic or aromatic bonds (C-C / C-H), carbon in ketone/aldehyde (C=O) or ether bonds (C-O-C), and carbon in carboxylic bonds (O=C-O), respectively[30-31]. Two peak fittings were performed for the O 1s peak, whose positions were at approx. 531 eV and 533 eV: the former peak corresponds to the oxygen in hydroxyl (-OH) groups and the latter is assigned to oxygen in O=C-O bonds[32-33]. By deconvolution of the N 1s peak, the selected peaks were assigned to nitrogen with pyridinic (ca. 398 eV) and pyrolic characteristics (ca. 400 eV)[34]. Finally, the S 2p peak was deconvoluted by using two-peak fittings at approx. 164 eV and 165 eV, which reflect thiophenic and sulfite characteristics, respectively[35]. The relative contents of each atom in different bonds can be estimated from the area under the sub-peaks. The detailed deconvolution data of each high-resolution peak are summarized in Table 3. It is observed that the carbon existed predominately in the form of aliphatic or aromatic bonds, which constructs the main molecular structure of

asphaltene. Most of the nitrogen atoms (75.44%) were pyrrolic bonding structures, which is in agreement with other studies on different asphaltene samples[36].

The morphology of asphaltene was characterized with SEM, which is provided in Figure S1 in Electronic Supplementary Information (ESI). The platelet-like asphaltene particles was in the hundreds of nanometers and they exhibited a stacked agglomeration caused by the strong self-aggregation propensity of the asphaltene molecules. A similar asphaltene morphology was also observed by F. Trejo *et al.*[37].

3.2. **Characterization of functionalized asphaltene**

Thermal stability of pristine and silane-modified asphaltene was examined by TGA. As shown in Figure 4, pristine asphaltene exhibited degradation at 300 °C, followed by a significant weight loss between 450 °C and 550 °C, where the maximum weight loss was observed at 503 °C, as indicated by the sharp peak in the differential thermal analysis (DTA) curve. The pyrolysis of pristine asphaltene showed similar thermal degradation behavior as asphaltenes examined in previous works[38-39]. Two silane-treated asphaltenes exhibited similar thermal degradation behavior as the pristine asphaltene molecules; however, they present an additional noticeable weight reduction at approx. 340 °C, as seen in the DTA curves, which was attributed to the decomposition of the silane coupling agents. Finally, 4.359 wt.% and 4.139 wt.% residual silica were left in the two silane modified asphaltenes after the pyrolysis process.

Figure 5(a) displays the XPS survey spectra of pristine and functionalized asphaltene. As expected, the spectra of both APTES and GPTMS treated asphaltene indicate the presence of silicon element. The changes in the relative portions of the different elements are quantified in Figure 5(b). Here it is seen that in addition to the increase in Si concentration by 2.75% and 2.45% for GPTMS- and APTES-treated asphaltene, the oxygen atomic concentration also doubled in

both silane-treated samples as the result of the introducing with extra oxygen atoms in the silane coupling agents during asphaltene molecular functionalization. In addition, APTES-treated asphaltene also displayed a slightly increasing amount of nitrogen content after amine functional groups ($-NH_2$) were successfully grafted onto the asphaltene molecules. Finally, the relative carbon content was reduced after the functionalization because the total number of heteroatoms (N%+O%+S%) increased in addition to the presence of Si.

Figure 6 compares the functionalization effect on bonding structures of asphaltene molecule. Specifically, as amine C-N binding energy position overlaps C=O / C-O-C bonds at ca. 286 eV[30], therefore APTES-treated sample exhibited a higher content of C-N bonds in Figure 6(a). The deconvolution of oxygen spectra in two silane treated asphaltene was based on the two peaks positions at ca. 532 and 534 eV, which corresponded to ether (C-O-C) and carboxylic moieties[40]. During the silanization reaction, due to the hydrolysable alkoxy groups ($-CH_3$) in both GPTMS and APTES turned into reactive silanol group (Si-OH) to react with hydroxyl or carboxyl moieties on asphaltene molecules, therefore in Figure 6(b), two treated fillers displayed the disappearance of hydroxyl group, a substantial diminishing in the amounts of carboxylic groups, and the presence of ether moiety. Figure 6(c) and (d) manifest that nitrogen and sulfur binding structures were not changed upon the functionalization with silanes. Lastly, due to no Si element was detected from pristine asphaltene, relative amount of different Si bonds (Si-O-C at 102 eV; Si-O-Si at 103 eV)[41] is compared among the two functionalized samples in Figure 6(e). It is found that both specimen contained higher numbers of Si-O-C bonding. The detailed deconvolution data is available in ESI Table S1.

FTIR was performed to compare pristine and functionalized asphaltene to further verify the silanization reaction between pristine asphaltene and APTES/GPTMS functionalized samples.

As shown in Figure 7, although the two silane-treated asphaltenes largely preserved the main characteristic peaks of the pristine samples in the FTIR spectra from Figure 1, they exhibited several additional peaks. Specifically, both APTES and GPTMS modified asphaltene displayed new peaks at 1095 and 1031 cm^{-1}, which can be assigned to poly(dimethylsiloxane) $[(CH_3)_2SiO]_x$[42-43]. Furthermore, the peak intensity between 865 to 750 cm^{-1} was higher than for pristine asphaltene, which was not caused by the changes in out-of-plane C-H bending in aromatic rings of the asphaltene, but by the presence of Si-CH_3 bonds in the polysiloxanes (approx. 1260, 865-750 cm^{-1}) after molecular functionalization.

3.3. **Characterization of asphaltene/epoxy composites**

In Figure 8(a), reinforcement effect of asphaltene is recognized from the gradually improving the storage modulus (E') of neat epoxy in both glassy and rubbery regions as polymer matrix incorporated by increasing fillers loading over the measuring temperature range. Figure 8(b) demonstrates the *tan δ* curve of epoxy composites reinforced with various loadings of asphaltene. Interestingly, no obvious change in either peak magnitude or peak position of *tan δ* was observed, suggesting that the incorporated asphaltene molecules exhibit good compatibility with the epoxy matrix during curing without exerting detrimental effects on crosslink density or glass transition temperature (T_g) of epoxy resin.

Figure 9(a) compares the E' of epoxy resin composites reinforced by untreated and functionalized asphaltene at room temperature. As expected, the storage modulus of all epoxy composites enhanced independent of the functionality of asphaltene with increasing loading levels. However, it is found that the composites containing functionalized asphaltene (both GPTMS and APTES) exhibited overall higher E' values than those reinforced with pristine

asphaltene. Specifically, the improvement of E' in APTES-treated asphaltene contained epoxy system is higher than the specimen incorporated with pristine filler (36% *vs.* 22%) at 3 wt. % loading; while, the highest enhancement (ca. 40%) is achieved by blending with GPTMS-treated filler at 5 wt. % compared with 28% increment of E' in pristine asphaltene/epoxy composites. This result suggests that: silane molecular modification of asphaltene facilitated the grafting of functional groups (e.g. epoxy and amine moieties) onto asphaltene structure, which improved the filler's compatibility in epoxy resin and intensified the filler/matrix interfacial interactions through the formation of covalent chemical bonds, thus led to a further reinforcement effect by presence of rigid microstructures within the polymer networks. Figure 9(b) also shows a slight increase in T_g for all epoxy composites compared to neat epoxy (141.6 °C). However, the increase in T_g did not exhibit a strong correlation to the functionalization or loadings of asphaltene.

Thermal stability of asphaltene/epoxy composites was studied under nitrogen atmosphere. Overall, both neat epoxy and asphaltene/epoxy composites exhibited similar thermal degradation behavior (see Figure S2(a)-(c) in ESI). Thermal stability of the samples was determined by using the temperature at 5% and 10% weight loss. As seen in Table 4, the incorporation of asphaltene had no deteriorating effect on the thermal stability of the epoxy resin, indicating the potential suitability of asphaltene/epoxy composites for high temperature applications.

4. Conclusion

In this work, asphaltene was extracted from asphalt *via* a SARA route. Different characterization techniques showed that this asphaltene was comprised of 6 to 7 benzene rings fused within a polyaromatic structure and it had a morphology resembling highly stacked, platelet-like

aggregations. Molecular functionalization of asphaltene with GPTMS and APTES silane coupling agents was performed and confirmed by XPS, TGA and FTIR analysis. The asphaltene/epoxy composites with four different loading levels were successfully prepared and their thermo-mechanical properties characterized. The reinforcing effect of asphaltene in the polymer matrix was recognized by a gradual increment in storage modulus of the epoxy composites with increasing filler level. Although the overall materials' cost and processing complexity might be higher by involving in the efforts of silane functionalization, the incorporation of functionalized asphaltenes into the epoxy resin resulted in a more pronounced increase in storage modulus attributing to the enhanced interfacial interaction with polymer matrix. In addition, the introduced asphaltene also slightly increased the glass transition temperature without detrimental effects on the thermal stability of the epoxy resin. In conclusion, the improvement of thermo-mechanical properties, the potential abundant reserves of the resources, and most importantly, the promising low cost make asphaltene an ideal filler material for scale-up efforts in the polymer composites industry.

Acknowledgement

The authors acknowledge funding for this project from Honeywell Federal Manufacturing & Technologies, LLC. The authors also acknowledge Dr. James Anderegg (Ames Laboratory) for his assistance with XPS measurements and Dr. Steve Veysey (Department of Chemistry, Iowa State University) for his assistance with the elemental analysis.

References

1. Silva, S. L.; Silva, A. M. S.; Ribeiro, J. C.; Martins, F. G.; Da Silva, F. A.; Silva, C. M., Chromatographic and spectroscopic analysis of heavy crude oil mixtures with emphasis in nuclear magnetic resonance spectroscopy: A review. *Anal. Chim. Acta* **2011,** *707* (1), 18-37.

2. Gentzis, T.; Rahimi, P. M., A microscopic approach to determine the origin and mechanism of coke formation in fractionation towers. *Fuel* **2003,** *82* (12), 1531-1540.
3. Bartholdy, J.; Andersen, S. I., Changes in asphaltene stability during hydrotreating. *Energy Fuels* **2000,** *14* (1), 52-55.
4. Alboudwarej, H.; Jakher, R. K.; Svrcek, W. Y.; Yarranton, H. W., Spectrophotometric measurement of asphaltene concentration. *Petroleum Science and Technology* **2004,** *22* (5-6), 647-664.
5. Painter, P. C.; Sobkowiak, M.; Youtcheff, J., FT-i.r. study of hydrogen bonding in coal. *Fuel* **1987,** *66* (7), 973-978.
6. Anisimov, M. A.; Yudin, I. K.; Nikitin, V.; Nikolaenko, G.; Chernoutsan, A.; Toulhoat, H.; Frot, D.; Briolant, Y., Asphaltene aggregation in hydrocarbon solutions studied by photon correlation spectroscopy. *J. Phys. Chem.* **1995,** *99* (23), 9576-9580.
7. Acevedo, S.; Méndez, B.; Rojas, A.; Layrisse, I.; Rivas, H., Asphaltenes and resins from the Orinoco basin. *Fuel* **1985,** *64* (12), 1741-1747.
8. Wilt, B. K.; Welch, W. T.; Rankin, J. G., Determination of asphaltenes in petroleum crude oils by fourier transform infrared spectroscopy. *Energy & Fuels* **1998,** *12* (5), 1008-1012.
9. Chiaberge, S.; Guglielmetti, G.; Montanari, L.; Salvalaggio, M.; Santolini, L.; Spera, S.; Cesti, P., Investigation of asphaltene chemical structural modification induced by thermal treatments. *Energy Fuels* **2009,** *23*, 4486-4495.
10. Wang, L.; Wang, K.; Chen, L.; Zhang, Y. W.; He, C. B., Preparation, morphology and thermal/mechanical properties of epoxy/nanoclay composite. *Compos. Pt. A-Appl. Sci. Manuf.* **2006,** *37* (11), 1890-1896.
11. Wang, W. S.; Chen, H. S.; Wu, Y. W.; Tsai, T. Y.; Chen-Yang, Y. W., Properties of novel epoxy/clay nanocomposites prepared with a reactive phosphorus-containing organoclay. *Polymer* **2008,** *49* (22), 4826-4836.
12. Iijima, M.; Sato, N.; Lenggoro, I. W.; Kamiya, H., Surface modification of BaTiO3 particles by silane coupling agents in different solvents and their effect on dielectric properties of BaTiO3/epoxy composites. *Colloid Surf. A-Physicochem. Eng. Asp.* **2009,** *352* (1-3), 88-93.
13. Yu, J. H.; Huang, X. Y.; Wu, C.; Wu, X. F.; Wang, G. L.; Jiang, P. K., Interfacial modification of boron nitride nanoplatelets for epoxy composites with improved thermal properties. *Polymer* **2012,** *53* (2), 471-480.
14. Wu, H. C.; Rogalski, M.; Kessler, M. R., Zirconium tungstate/epoxy nanocomposites: effect of nanoparticle morphology and negative thermal expansivity. *ACS Appl. Mater. Interfaces* **2013,** *5* (19), 9478-9487.
15. Wang, X. M.; Guo, J. J.; Yang, X. W.; Xu, B. S., Monodisperse carbon microspheres synthesized from asphaltene. *Materials Chemistry and Physics* **2009,** *113* (2-3), 821-823.
16. Natarajan, A.; Mahavadi, S. C.; Natarajan, T. S.; Masliyah, J. H.; Xu, Z. H., Preparation of solid and hollow asphaltene fibers by single step electrospinning. *J. Eng. Fiber Fabr.* **2011,** *6* (2), 1-6.
17. Christopher, J.; Sarpal, A. S.; Kapur, G. S.; Krishna, A.; Tyagi, B. R.; Jain, M. C.; Jain, S. K.; Bhatnagar, A. K., Chemical structure of bitumen-derived asphaltenes by nuclear magnetic resonance spectroscopy and X-ray diffractometry. *Fuel* **1996,** *75* (8), 999-1008.
18. Herrera, N. N.; Letoffe, J. M.; Putaux, J. L.; David, L.; Bourgeat-Lami, E., Aqueous dispersions of silane-functionalized laponite clay platelets. A first step toward the elaboration of water-based polymer/clay nanocomposites. *Langmuir* **2004,** *20* (5), 1564-1571.

19. Ma, P. C.; Kim, J. K.; Tang, B. Z., Effects of silane functionalization on the properties of carbon nanotube/epoxy nanocomposites. *Compos. Sci. Technol.* **2007,** *67* (14), 2965-2972.
20. Ma, D. L.; Hugener, T. A.; Siegel, R. W.; Christerson, A.; Martensson, E.; Onneby, C.; Schadler, L. S., Influence of nanoparticle surface modification on the electrical behaviour of polyethylene nanocomposites. *Nanotechnology* **2005,** *16* (6), 724-731.
21. Chrissopoulou, K.; Altintzi, I.; Anastasiadis, S. H.; Giannelis, E. P.; Pitsikalis, M.; Hadjichristidis, N.; Theophilou, N., Controlling the miscibility of polyethylene/layered silicate nanocomposites by altering the polymer/surface interactions. *Polymer* **2005,** *46* (26), 12440-12451.
22. Zhang, S. W.; Zhou, S. X.; Weng, Y. M.; Wu, L. M., Synthesis of SiO2/polystyrene nanocomposite particles via miniemulsion polymerization. *Langmuir* **2005,** *21* (6), 2124-2128.
23. Gu, J. W.; Zhang, Q. Y.; Dang, J.; Xie, C., Thermal conductivity epoxy resin composites filled with boron nitride. *Polym. Adv. Technol.* **2012,** *23* (6), 1025-1028.
24. Yen, T. F.; Wu, W. H.; Chilingar, G. V., A study of the structure of petroleum asphaltenes and related substances by proton nuclear magnetic resonance. *Energy Sources* **1984,** *7* (3), 275-304.
25. Fossen, M.; Kallevik, H.; Knudsen, K. D.; Sjoblom, J., Asphaltenes precipitated by a two-Step precipitation procedure. 2. Physical and chemical characteristics. *Energy Fuels* **2011,** *25* (8), 3552-3567.
26. Mouazen, M.; Poulesquen, A.; Vergnes, B., Influence of thermomechanical history on chemical and rheological behavior of bitumen. *Energy Fuels* **2011,** *25* (10), 4614-4621.
27. Bouhadda, Y.; Bormann, D.; Sheu, E.; Bendedouch, D.; Krallafa, A.; Daaou, M., Characterization of Algerian Hassi-Messaoud asphaltene structure using Raman spectrometry and X-ray diffraction. *Fuel* **2007,** *86* (12-13), 1855-1864.
28. Abdallah, W. A.; Yang, Y., Raman spectrum of asphaltene. *Energy Fuels* **2012,** *26* (11), 6888-6896.
29. Tuinstra, F.; Koenig, J. L., Raman spectroscopy of graphite**.** *J. Chem. Phys.* **1970,** *53* (3), 1126-1127.
30. Ramanathan, T.; Fisher, F. T.; Ruoff, R. S.; Brinson, L. C., Amino-functionalized carbon nanotubes for binding to polymers and biological systems. *Chem. Mater.* **2005,** *17* (6), 1290-1295.
31. Huang, Y.-L.; Tien, H.-W.; Ma, C.-C. M.; Yang, S.-Y.; Wu, S.-Y.; Liu, H.-Y.; Mai, Y.-W., Effect of extended polymer chains on properties of transparent graphene nanosheets conductive film. *J. Mater. Chem.* **2011,** *21* (45), 18236-18241.
32. Beamson, G.; Briggs, D., High resolution monochromated X-ray photoelectron spectroscopy of organic polymers: A comparison between solid state data for organic polymers and gas phase data for small molecules. *Mol. Phys.* **1992,** *76* (4), 919-936.
33. Wang, J. Q.; Li, C.; Zhang, L. L.; Que, G. H.; Li, Z. M., The properties of asphaltenes and their interaction with amphiphiles. *Energy Fuels* **2009,** *23* (7), 3625-3631.
34. Kelemen, S. R.; Gorbaty, M. L.; Kwiatek, P. J., Quantification of nitrogen forms in Argonne premium coals. *Energy Fuels* **1994,** *8* (4), 896-906.
35. Abdallah, W. A.; Taylor, S. D., Surface characterization of adsorbed asphaltene on a stainless steel surface. *Nucl. Instrum. Methods Phys. Res. Sect. B-Beam Interact. Mater. Atoms* **2007,** *258* (1), 213-217.

36. Siskin, M.; Kelemen, S. R.; Eppig, C. P.; Brown, L. D.; Afeworki, M., Asphaltene molecular structure and chemical influences on the morphology of coke produced in delayed coking. *Energy Fuels* **2006,** *20* (3), 1227-1234.
37. Trejo, F.; Ancheyta, J.; Rana, M. S., Structural characterization of asphaltenes obtained from hydroprocessed crude oils by SEM and TEM. *Energy Fuels* **2009,** *23* (1), 429-439.
38. Murugan, P.; Mahinpey, N.; Mani, T., Thermal cracking and combustion kinetics of asphaltenes derived from Fosterton oil. *Fuel Process. Technol.* **2009,** *90* (10), 1286-1291.
39. Murugan, P.; Mani, T.; Mahinpey, N.; Asghari, K., The low temperature oxidation of Fosterton asphaltenes and its combustion kinetics. *Fuel Process. Technol.* **2011,** *92* (5), 1056-1061.
40. Boudou, J. P.; Paredes, J. I.; Cuesta, A.; Martinez-Alonso, A.; Tascon, J. M. D., Oxygen plasma modification of pitch-based isotropic carbon fibres. *Carbon* **2003,** *41* (1), 41-56.
41. Vennerberg, D.; Rueger, Z.; Kessler, M. R., Effect of silane structure on the properties of silanized multiwalled carbon nanotube-epoxy nanocomposites. *Polymer* **2014,** *55* (7), 1854-1865.
42. A. Lee Smith, *Analysis of Silicones*. New York, **1974**.
43. Bellamy, L. J., *The Infra-red Spectra of Complex Molecules*. London, **1975**.

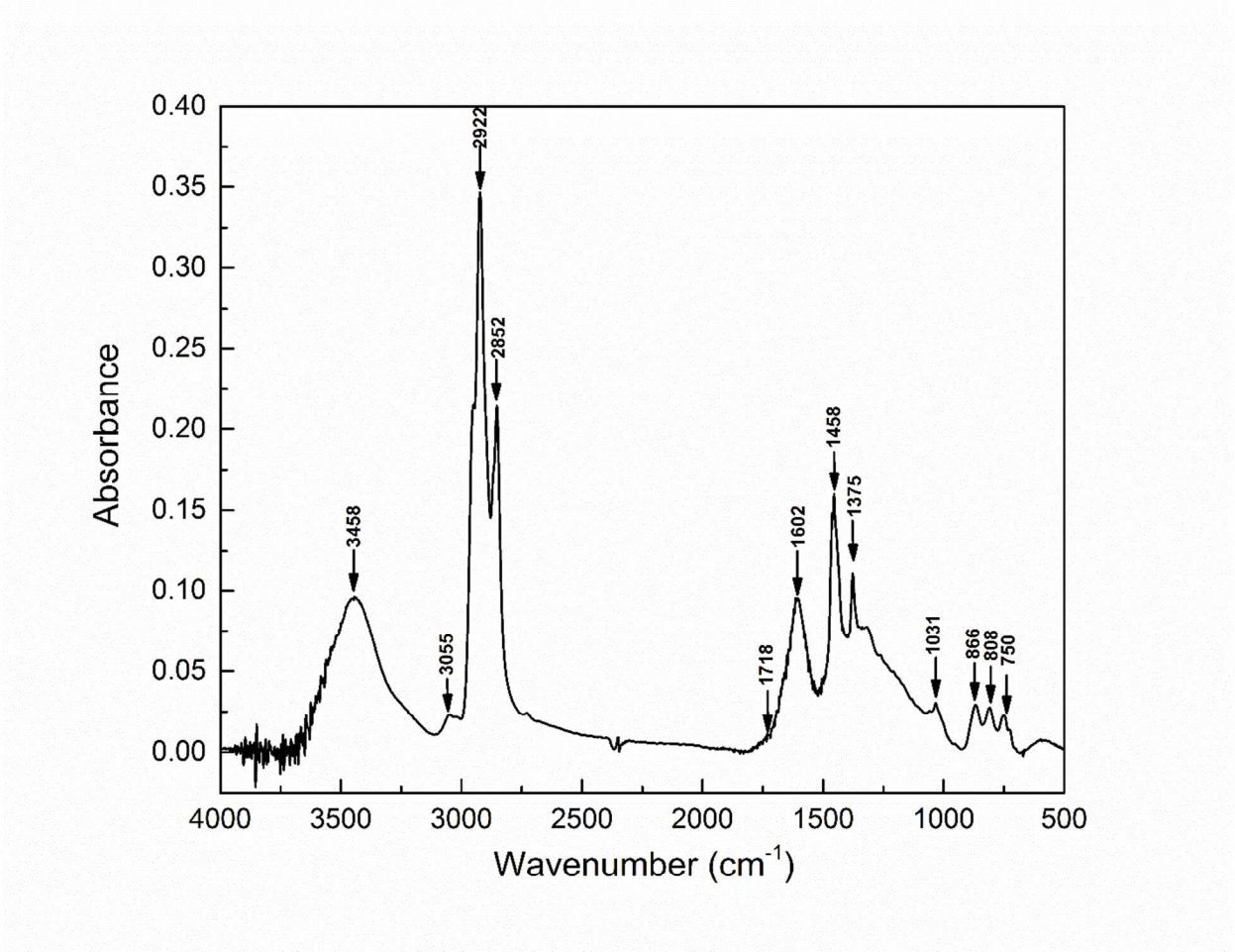

Figure 1. Main absorbance peaks in FTIR spectrum of asphaltene

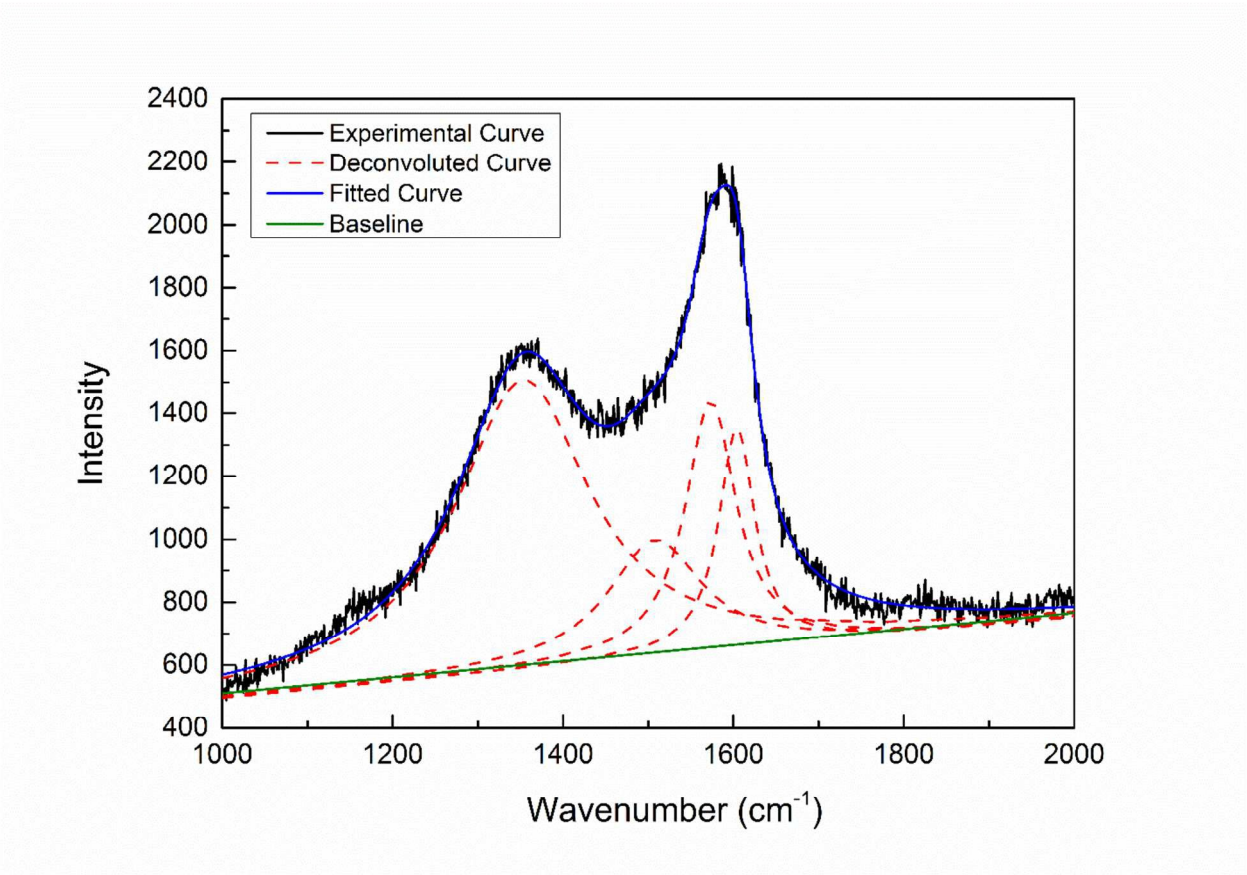

Figure 2. Deconvolution of experimental Raman spectra of asphaltene

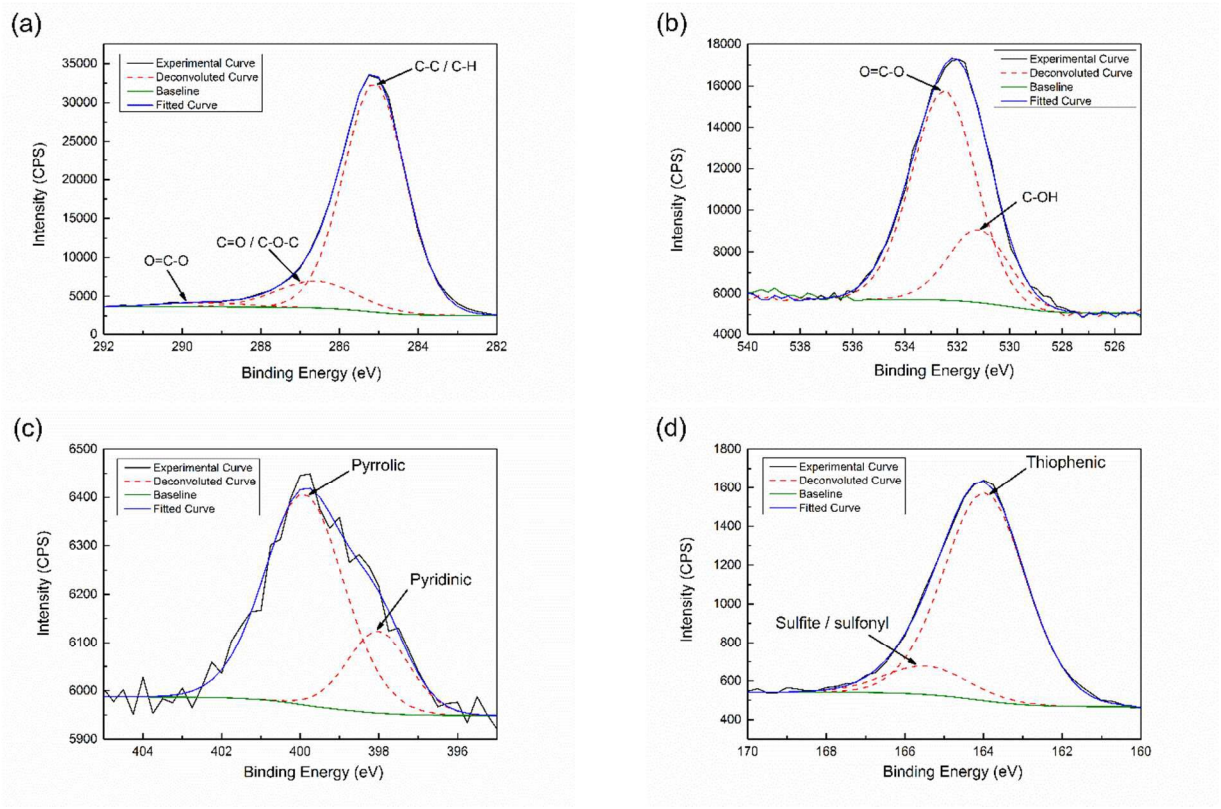

Figure 3. High-resolution XPS spectra with fitting of (a) C 1s, (b) O 1s, (c) N 1s, and (d) S 2p in asphaltene samples

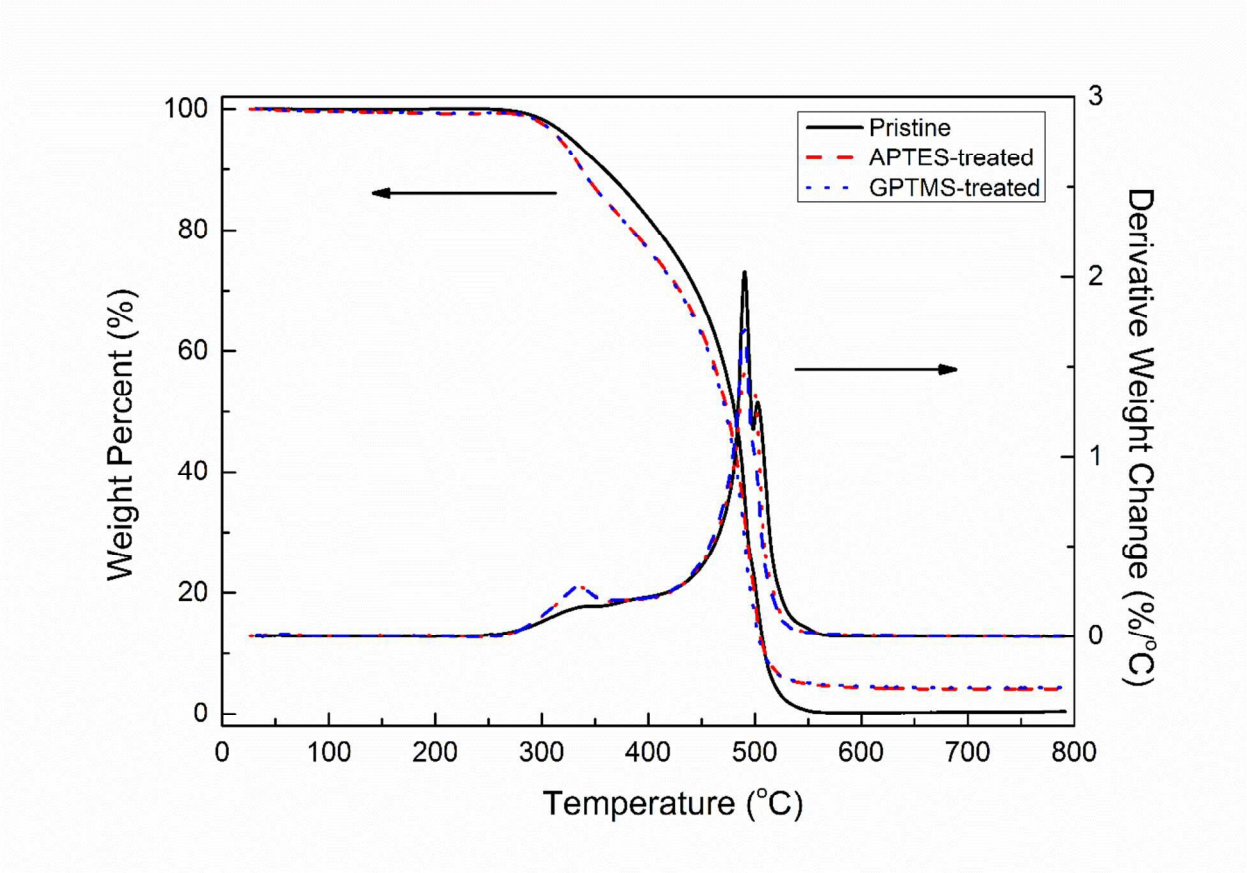

Figure 4. Comparison of thermal degradation of pristine and functionalized asphaltene in air

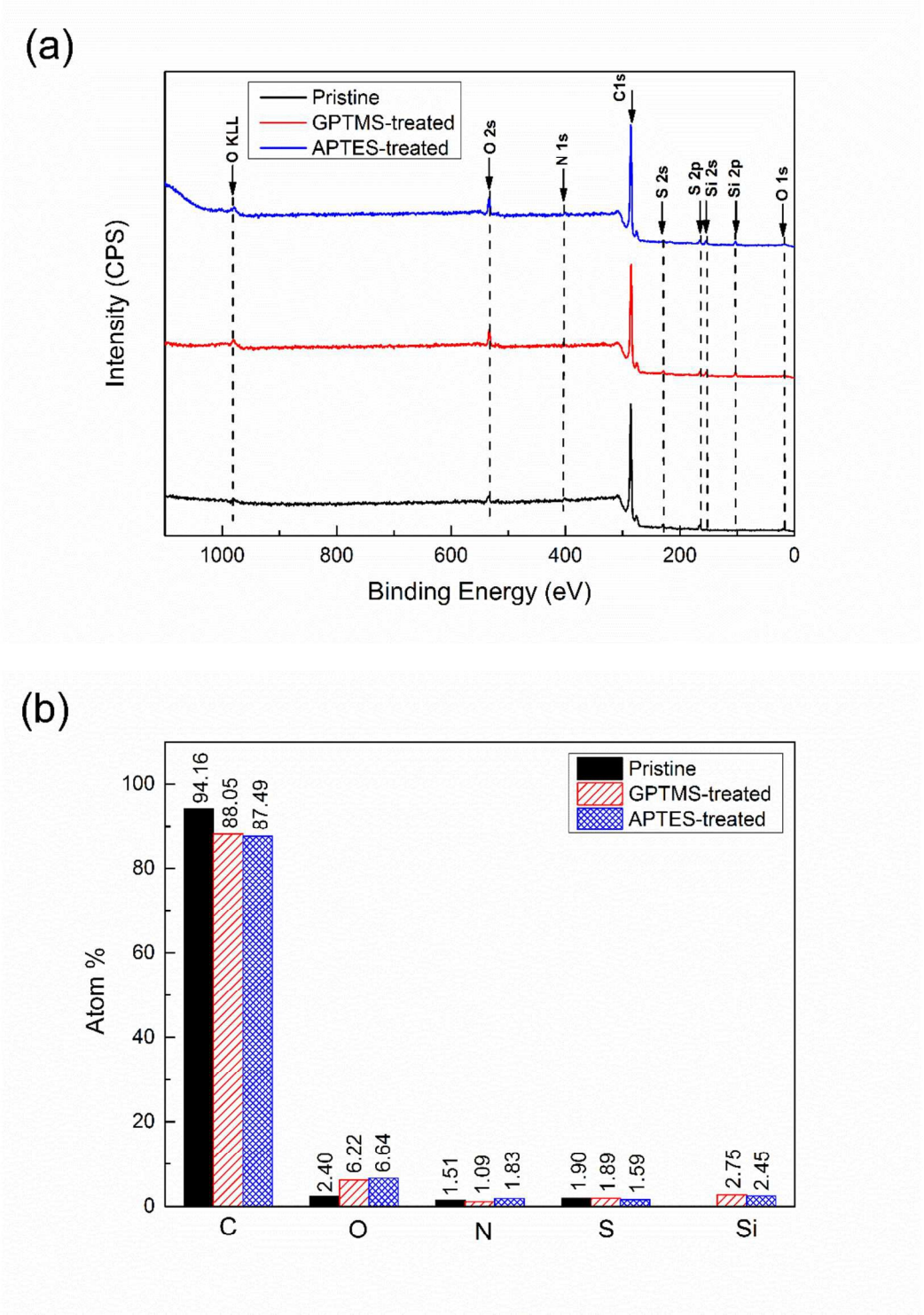

Figure 5. (a) XPS survey spectra and (b) atomic concentration comparison of pristine and functionalized asphaltene

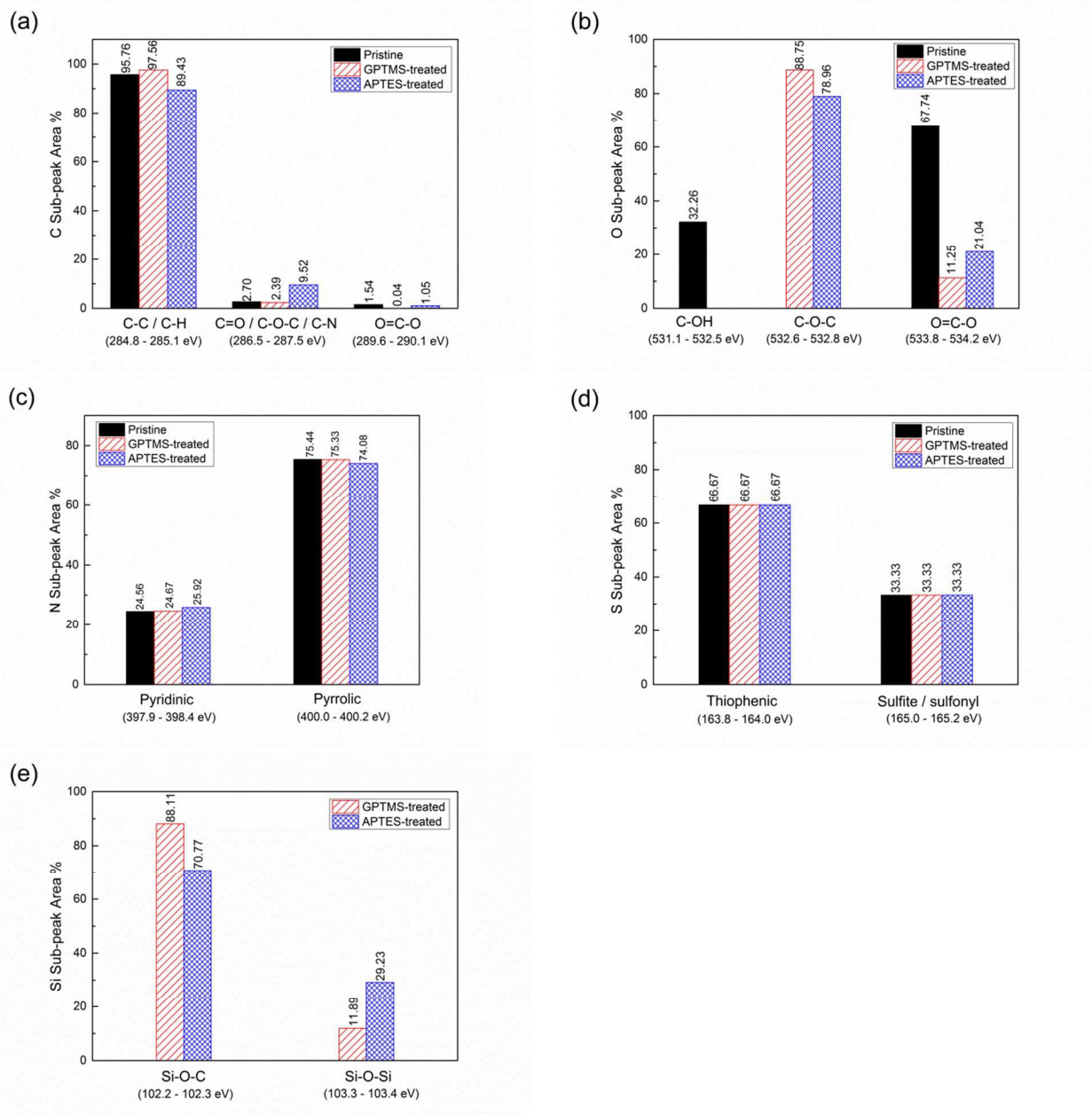

Figure 6. Comparison of different element binding types between pristine and treated asphaltene based on spectra deconvolution: (a) C 1s, (b) O 1s, (c) N 1s, (d) S 2p; and (e) Si 2p

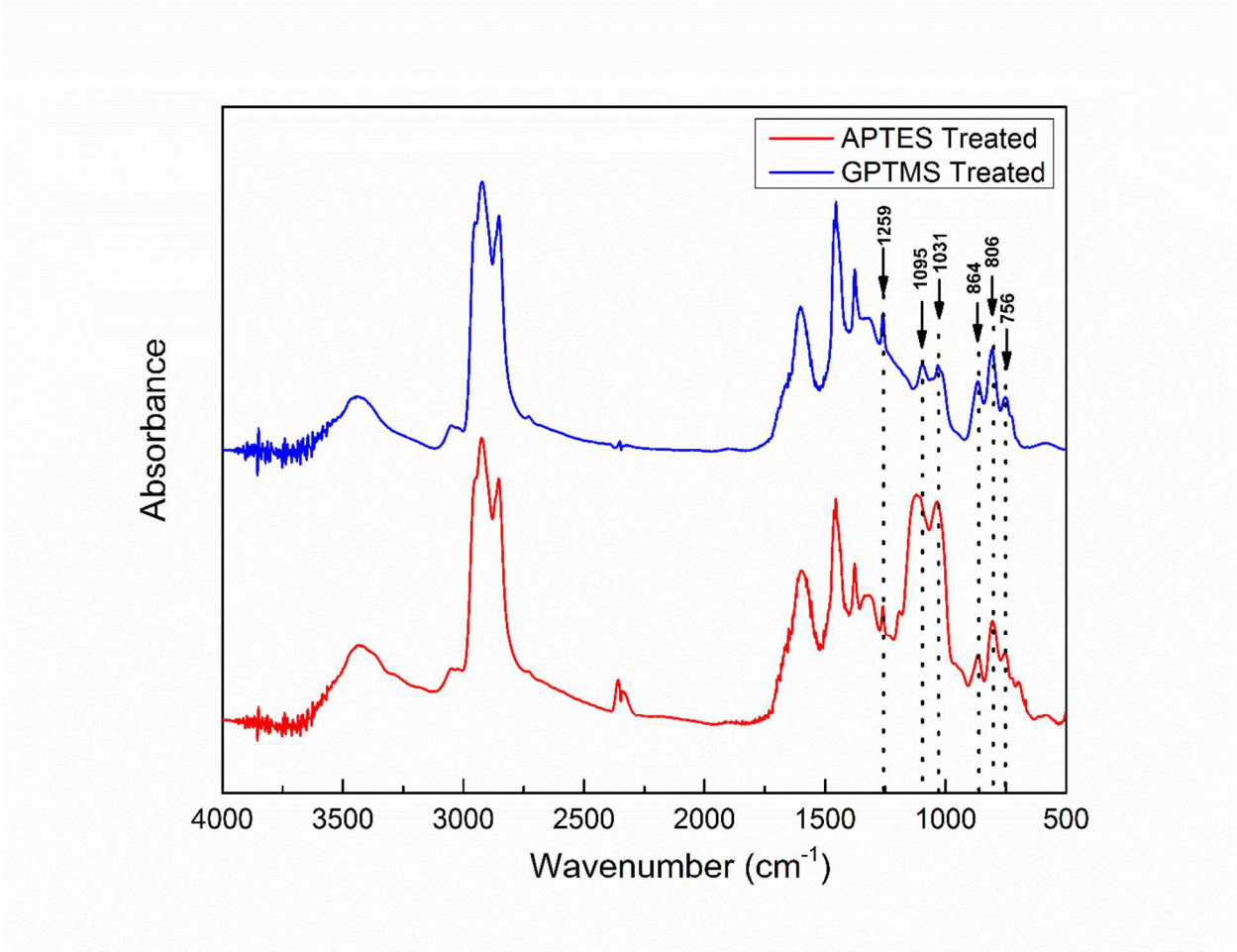

Figure 7. FTIR spectra of APTES- and GPTMS-treated asphaltene

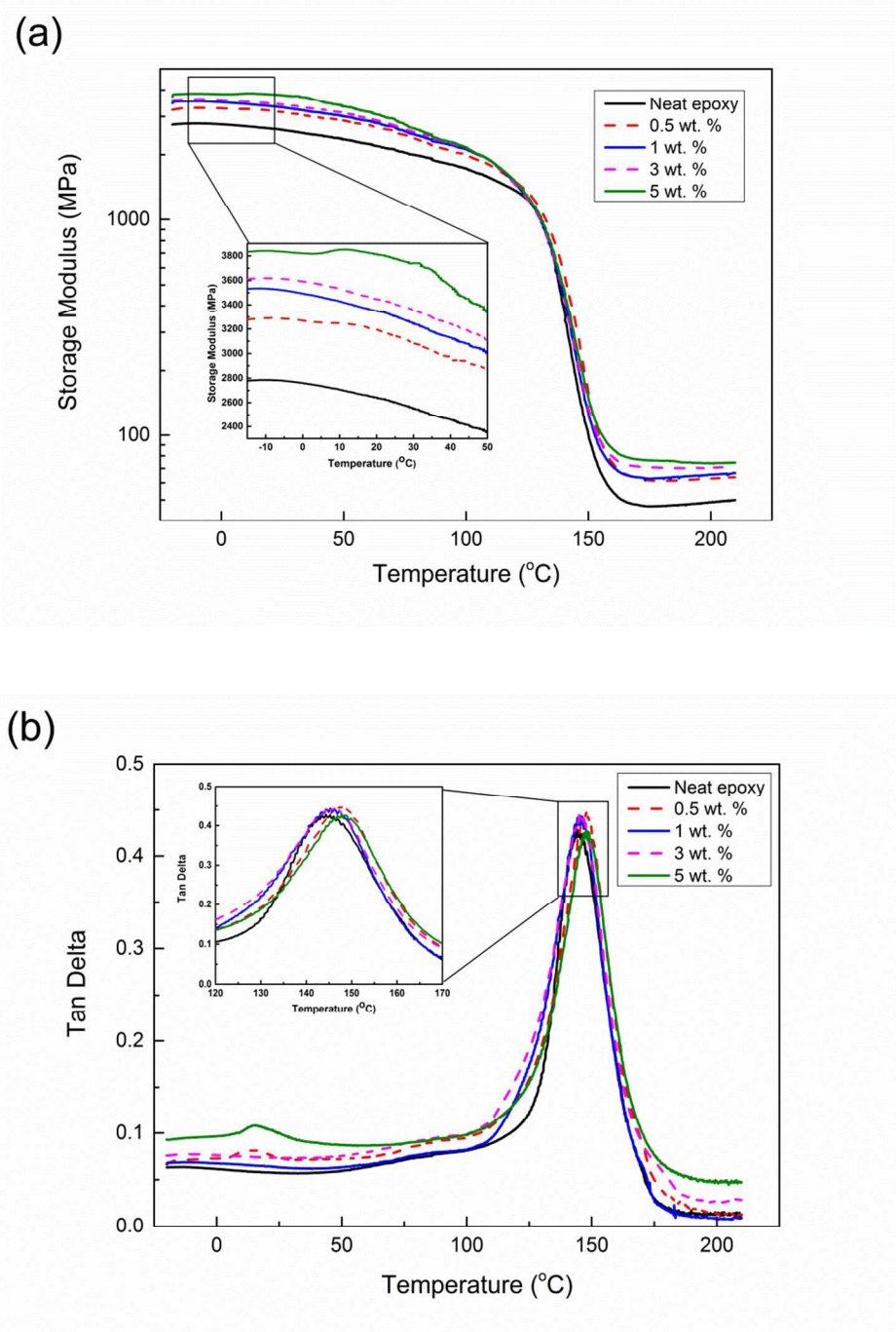

Figure 8. (a) Storage modulus (E') and (b) tan δ of epoxy composites reinforced by GPTMS-treated asphaltene at different loading levels

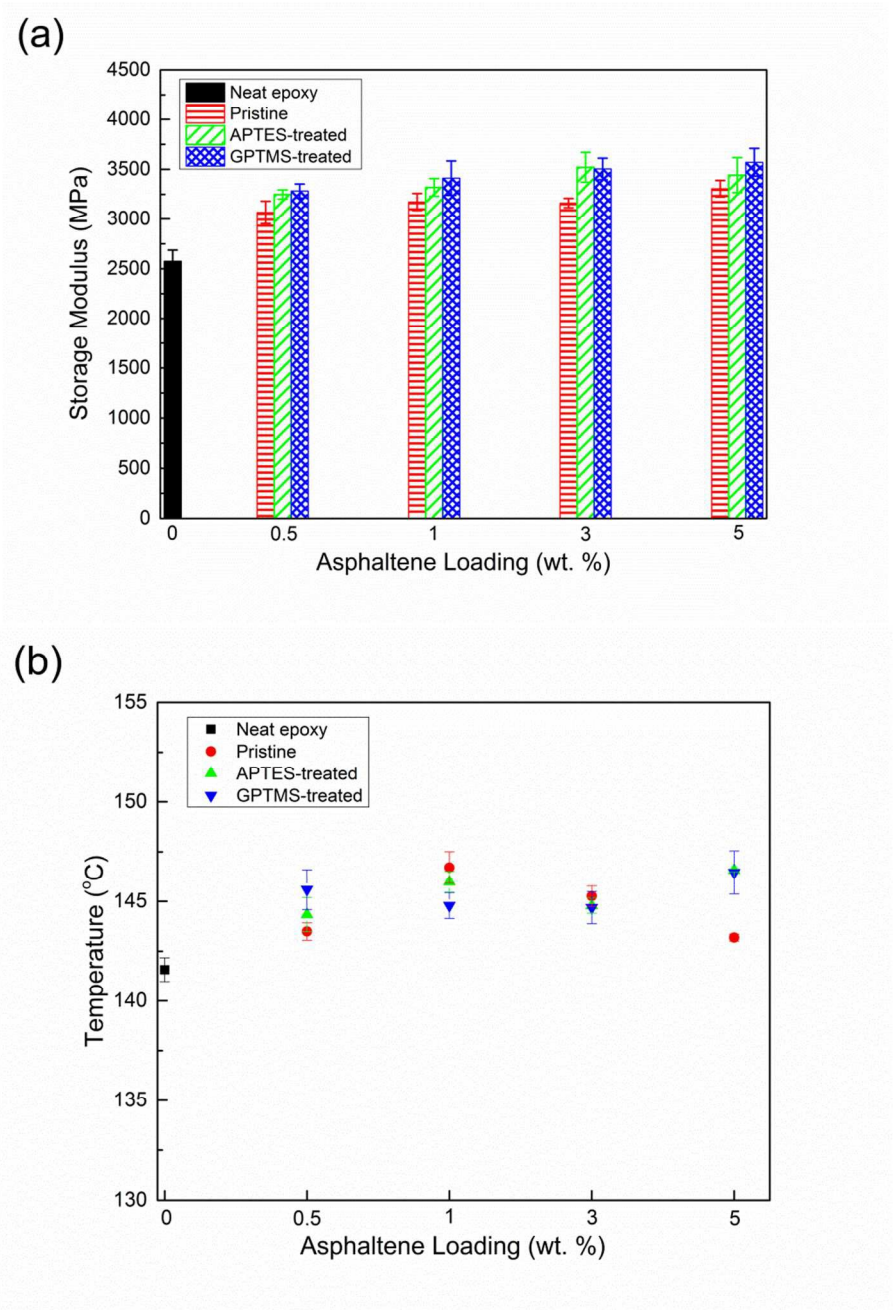

Figure 9. Comparison of (a) storage modulus (E') at 25 °C and (b) T_g of asphaltene/epoxy composites

Table 1. Elemental analysis of asphaltene

C (%)	84.245 ± 0.208
H (%)	7.682 ± 0.142
N (%)	1.395 ± 0.034
S (%)	5.690 ± 0.164
O* (%)	0.988 ± 0.121
H/C	1.094
(N+S+O)/C	0.0483

* Oxygen content was determined from the weight balance

Table 2. Summary of Raman spectra analysis of asphaltene

Band	Band position (cm^{-1})	FWHM (cm^{-1})	L_a (nm)	Numbers of aromatic rings
D1	1349.028 ± 2.270	175.201 ± 11.907	1.74 ± 0.097	6~7
D3	1497.022 ± 11.904	161.033 ± 47.903		
G	1569.117 ± 4.496	74.918 ± 3.901		
D2	1600.966 ± 2.669	54.773 ± 4.983		

Table 3. Deconvoluted peak data of high-resolution spectra of elements in pristine asphaltene

	Atomic concentration (%)	Position (eV)	FWHM (eV)	Area	%Area	Bond assignments
C 1s	94.16	284.78	2.04	79647	95.76	C-C
		287.05	2.01	2242	2.70	C-O-C
		289.93	2.09	1281	1.54	O=C-O
O 1s	2.40	531.16	2.46	1228	32.26	C-OH
		533.27	2.80	2578	67.74	O=C-O
N 1s	1.51	398.12	2.32	506	24.56	Pyridinic
		400.03	2.52	1553	75.44	Pyrrolic
S 2p	1.90	163.80	1.90	2462	66.67	Thiophenic
		165.00	2.10	1231	33.33	Sulfite or sulfonyl

Table 4. Thermal degradation temperatures of asphaltene/epoxy composites at 5% and 10% weight loss. The standard deviation was determined from four tested samples

Sample		Temperature at weight loss (°C)	
		5 wt. %	**10 wt. %**
Neat epoxy		345.56 ± 4.01	361.14 ± 2.47
0.5 wt.% asphaltene	Pristine	348.83 ± 2.50	362.51 ± 0.98
	APTES-treated	350.54 ± 2.04	363.64 ± 1.11
	GPTMS-treated	349.36 ± 2.38	362.34 ± 1.69
1 wt.% asphaltene	Pristine	353.58 ± 2.40	370.59 ± 1.25
	APTES-treated	350.37 ± 1.12	363.61 ± 0.66
	GPTMS-treated	351.34 ± 1.54	363.31 ± 1.36
3 wt.% asphaltene	Pristine	362.54 ± 0.67	374.10 ± 0.61
	APTES-treated	347.62 ± 0.65	361.96 ± 1.01
	GPTMS-treated	352.22 ± 2.14	364.48 ± 1.80
5 wt.% asphaltene	Pristine	347.68 ± 1.42	360.86 ± 1.17
	APTES-treated	350.90 ± 2.04	362.14 ± 1.79
	GPTMS-treated	350.70 ± 2.11	362.74 ± 1.21

Table of Content

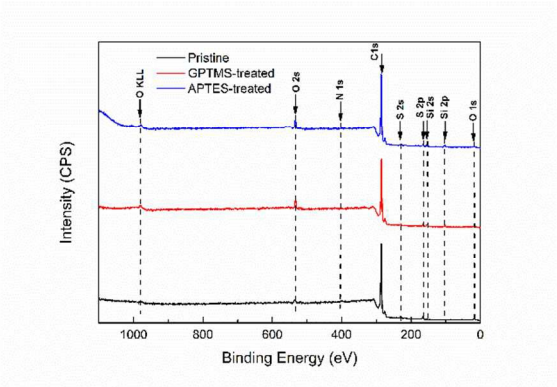

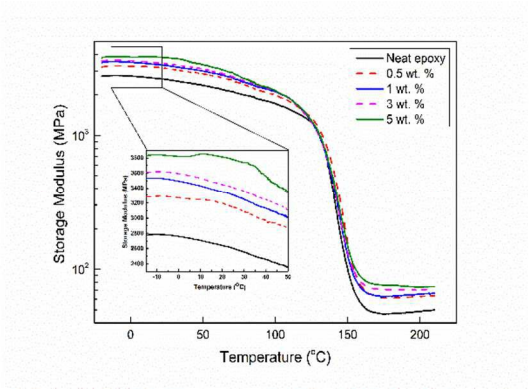

First comprehensive study focuses on extraction, characterization and functionalization of asphaltene as novel low-cost carbonaceous filler in epoxy resin.

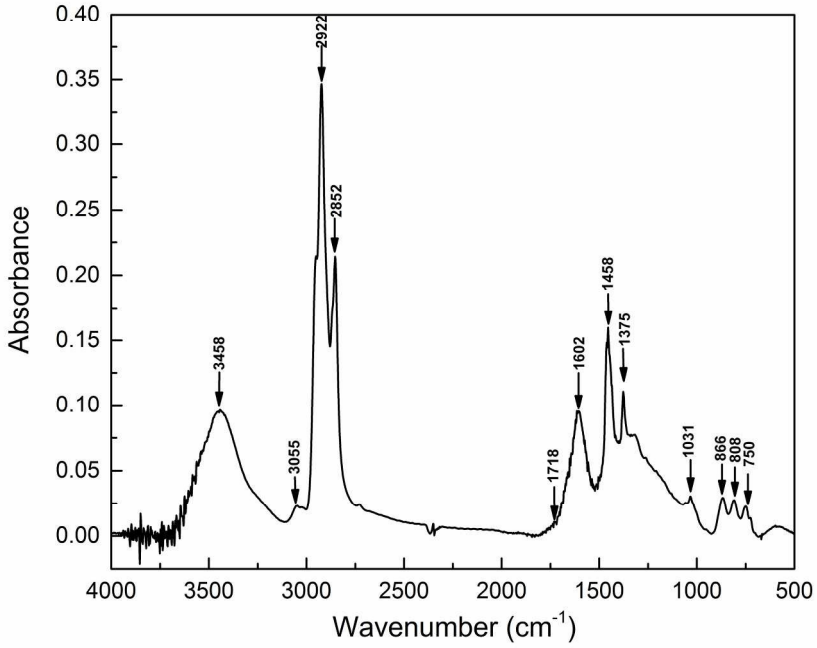

Figure 1. Main absorbance peaks in FTIR spectrum of asphaltene
215x166mm (300 x 300 DPI)

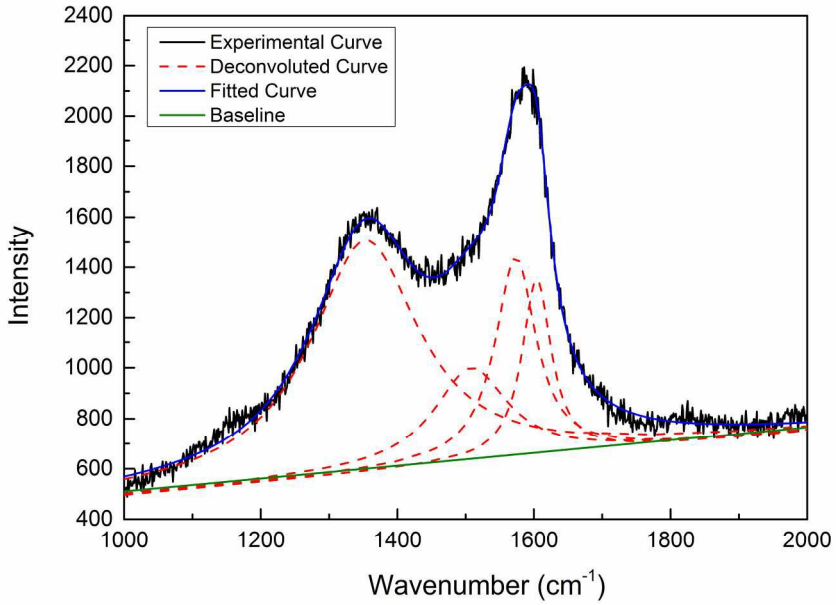

Figure 2. Deconvolution of experimental Raman spectra of asphaltene
201x141mm (300 x 300 DPI)

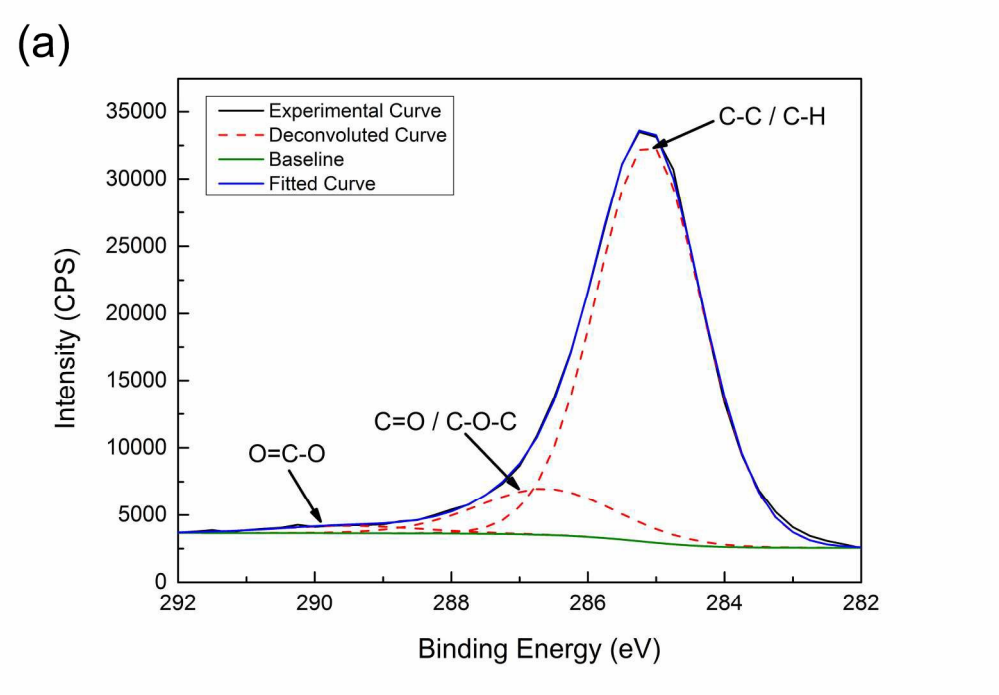

Figure 3. High-resolution XPS spectra with fitting of (a) C 1s, (b) O 1s, (c) N 1s, and (d) S 2p in asphaltene samples
201x141mm (300 x 300 DPI)

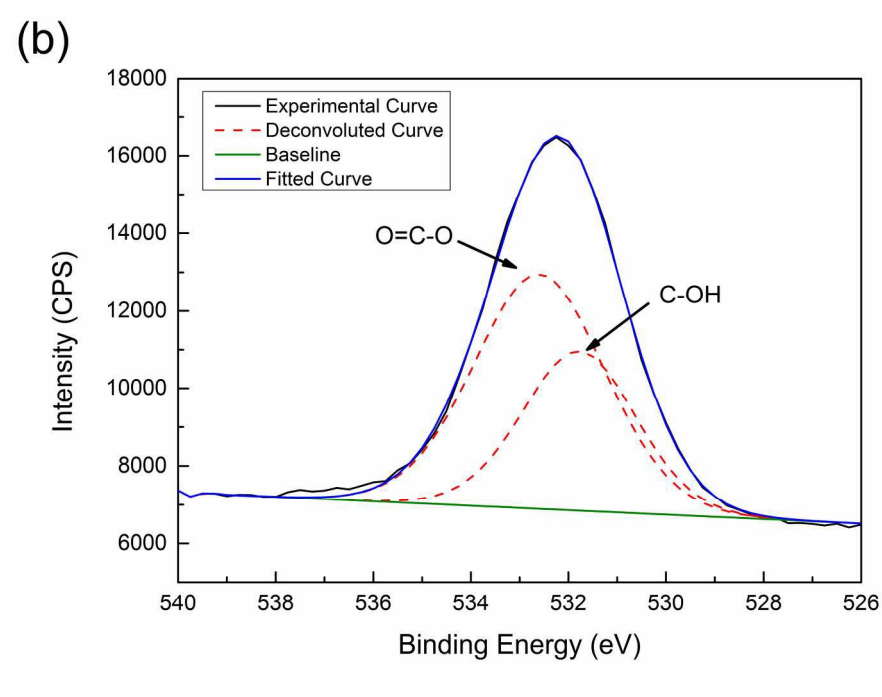

201x141mm (300 x 300 DPI)

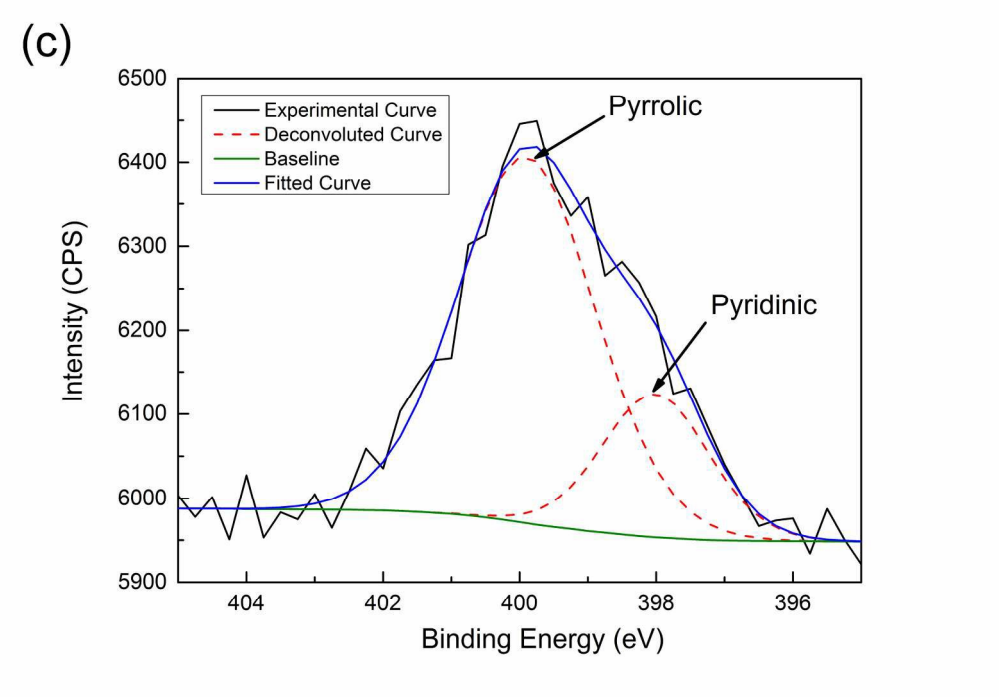

Figure 3. High-resolution XPS spectra with fitting of (a) C 1s, (b) O 1s, (c) N 1s, and (d) S 2p in asphaltene samples
201x141mm (300 x 300 DPI)

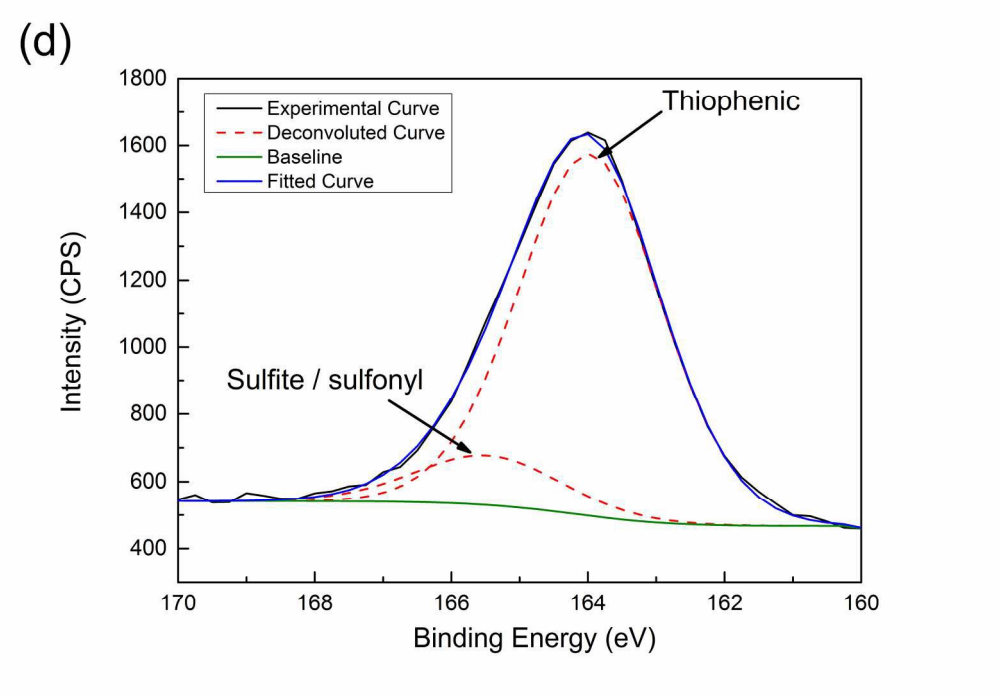

Figure 3. High-resolution XPS spectra with fitting of (a) C 1s, (b) O 1s, (c) N 1s, and (d) S 2p in asphaltene samples
201x141mm (300 x 300 DPI)

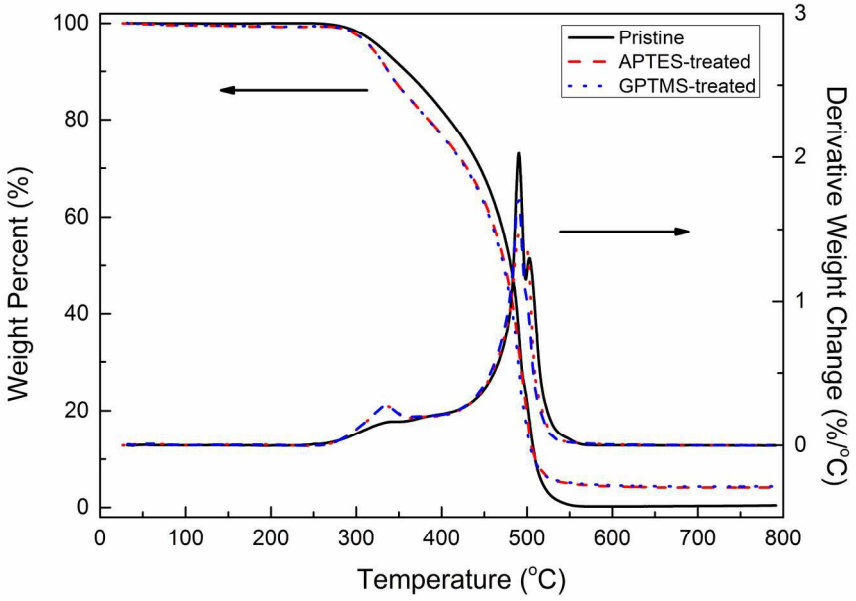

Figure 4. Comparison of thermal degradation of pristine and functionalized asphaltene in air
201x141mm (300 x 300 DPI)

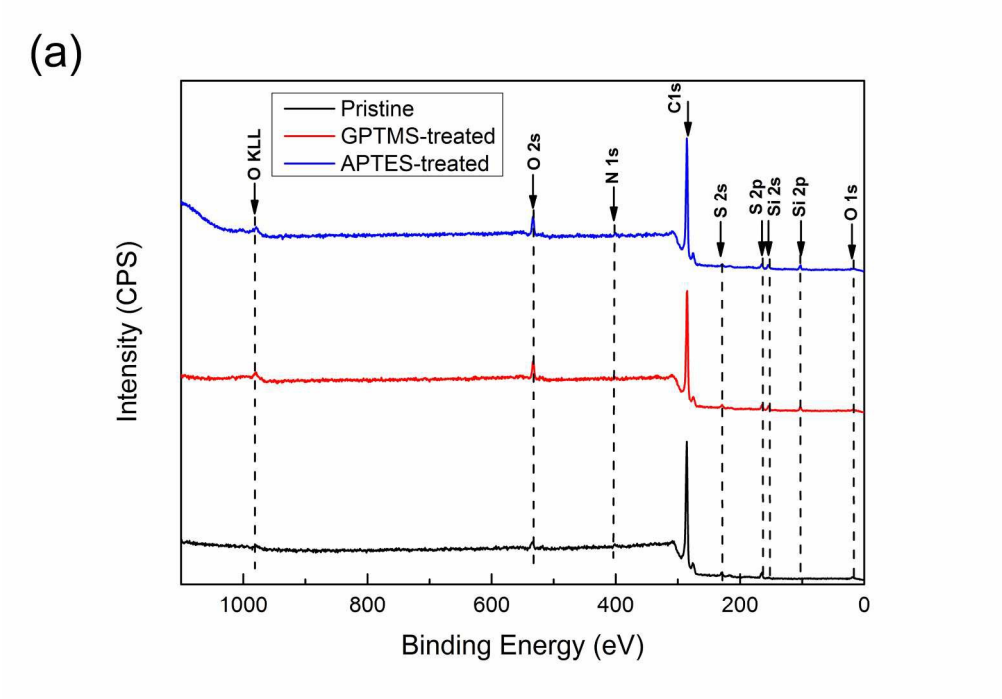

Figure 5. (a) XPS survey spectra and (b) atomic concentration comparison of pristine and functionalized asphaltene
201x141mm (300 x 300 DPI)

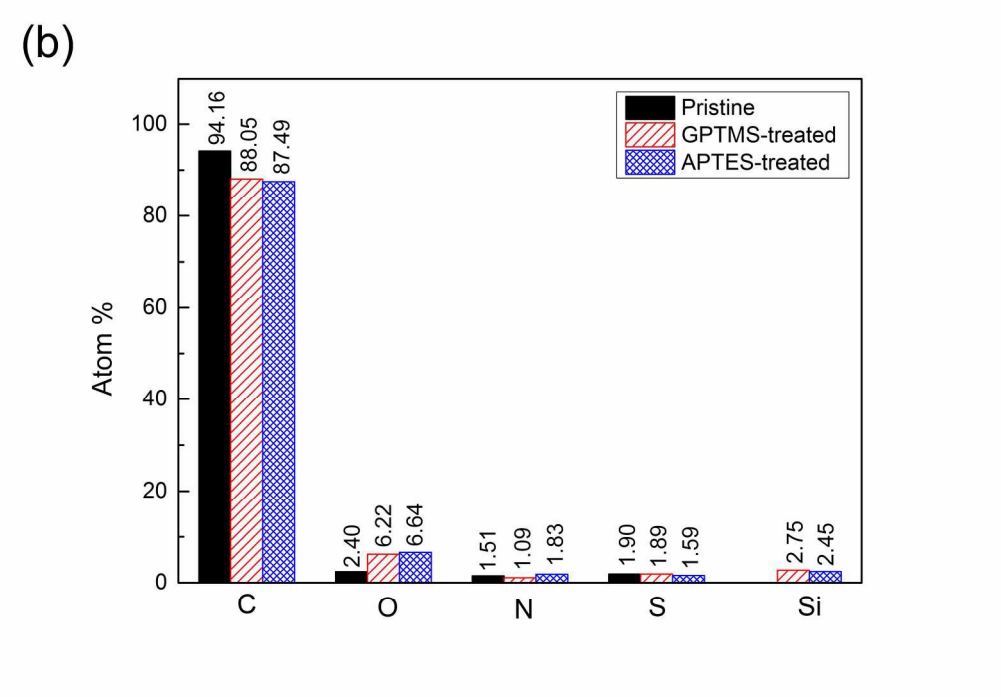

Figure 5. (a) XPS survey spectra and (b) atomic concentration comparison of pristine and functionalized asphaltene
201x141mm (300 x 300 DPI)

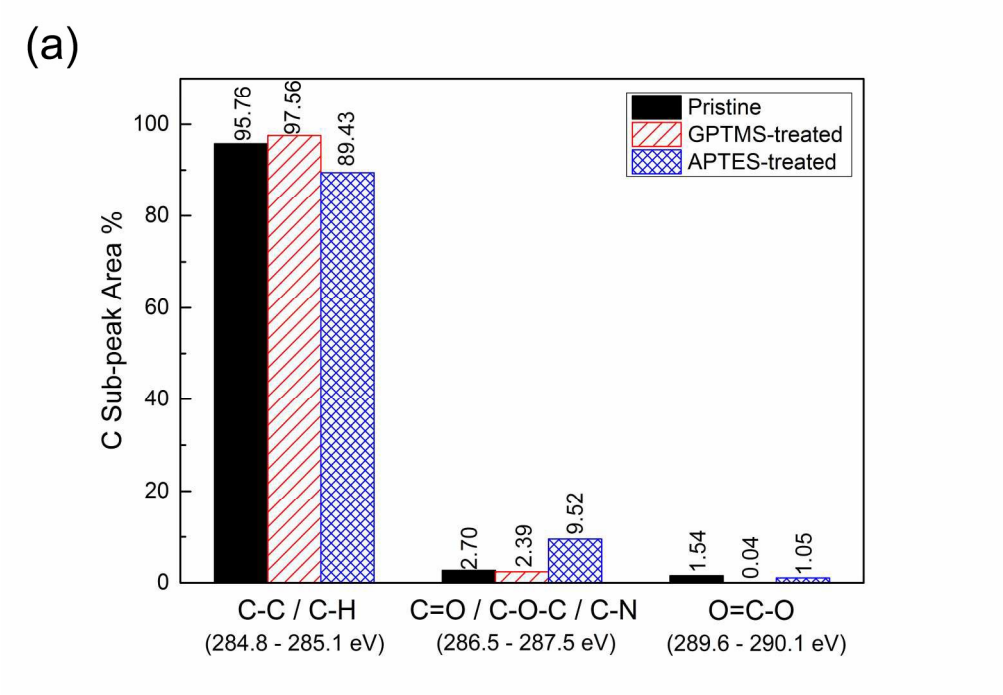

Figure 6. Comparison of different element binding types between pristine and treated asphaltene based on spectra deconvolution: (a) C 1s, (b) O 1s, (c) N 1s, (d) S 2p; and (e) Si 2p
201x141mm (300 x 300 DPI)

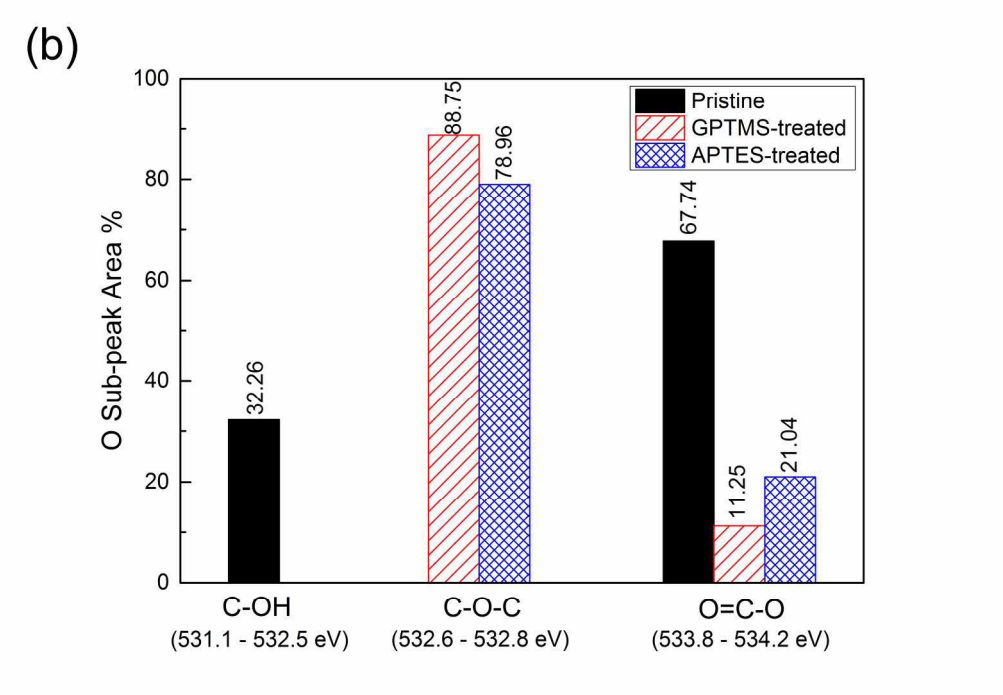

Figure 6. Comparison of different element binding types between pristine and treated asphaltene based on spectra deconvolution: (a) C 1s, (b) O 1s, (c) N 1s, (d) S 2p; and (e) Si 2p
201x141mm (300 x 300 DPI)

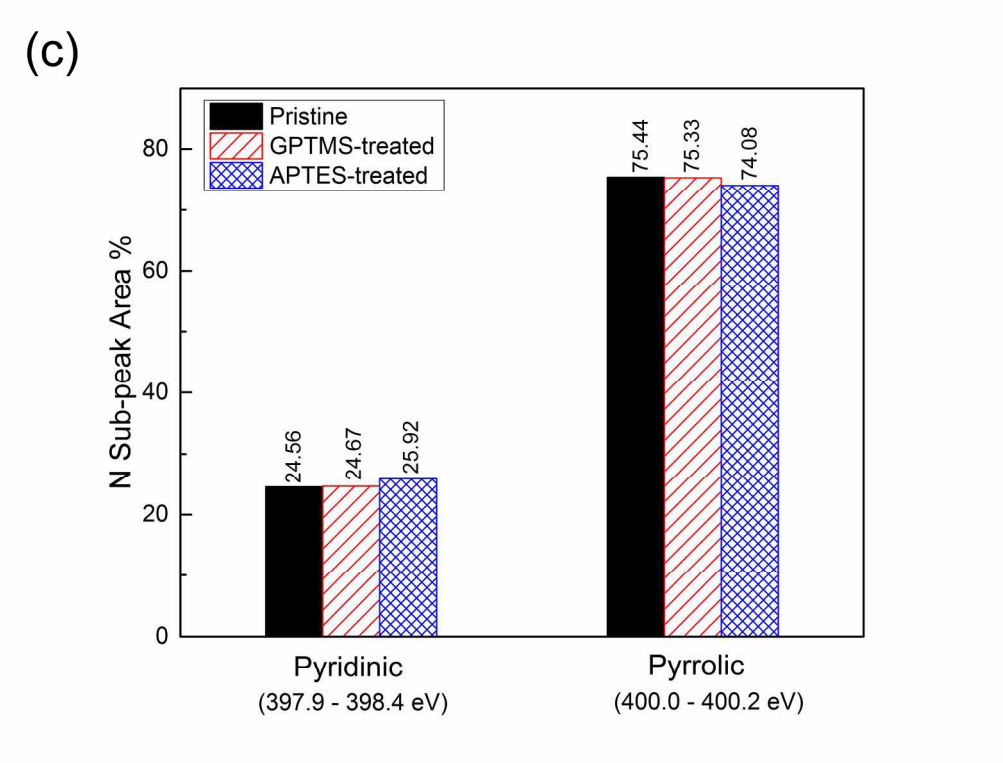

Figure 6. Comparison of different element binding types between pristine and treated asphaltene based on spectra deconvolution: (a) C 1s, (b) O 1s, (c) N 1s, (d) S 2p; and (e) Si 2p
205x157mm (300 x 300 DPI)

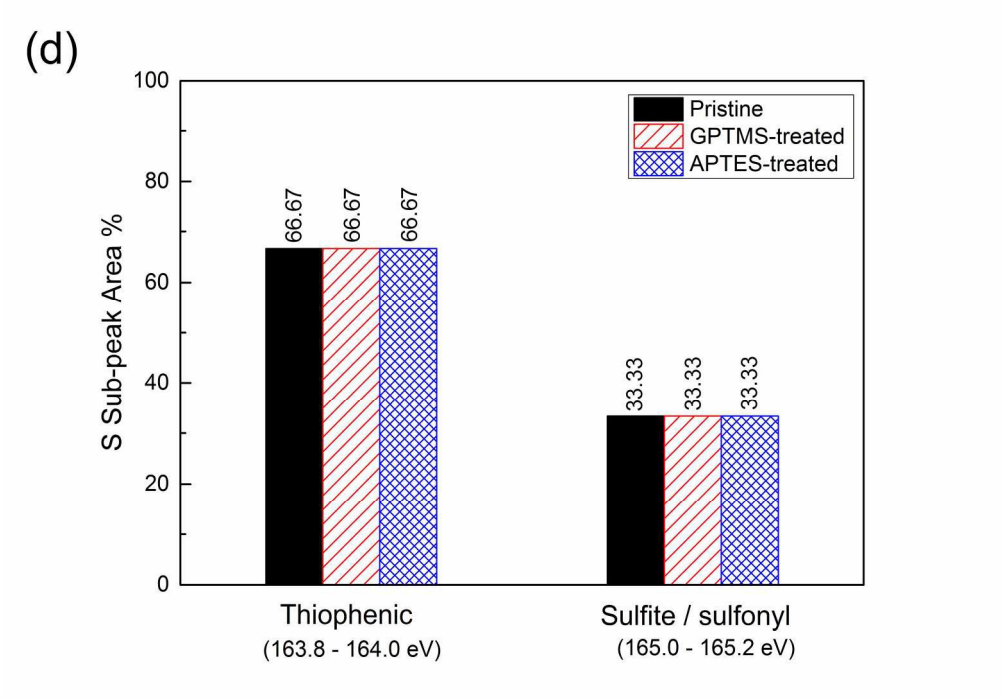

Figure 6. Comparison of different element binding types between pristine and treated asphaltene based on spectra deconvolution: (a) C 1s, (b) O 1s, (c) N 1s, (d) S 2p; and (e) Si 2p
201x141mm (300 x 300 DPI)

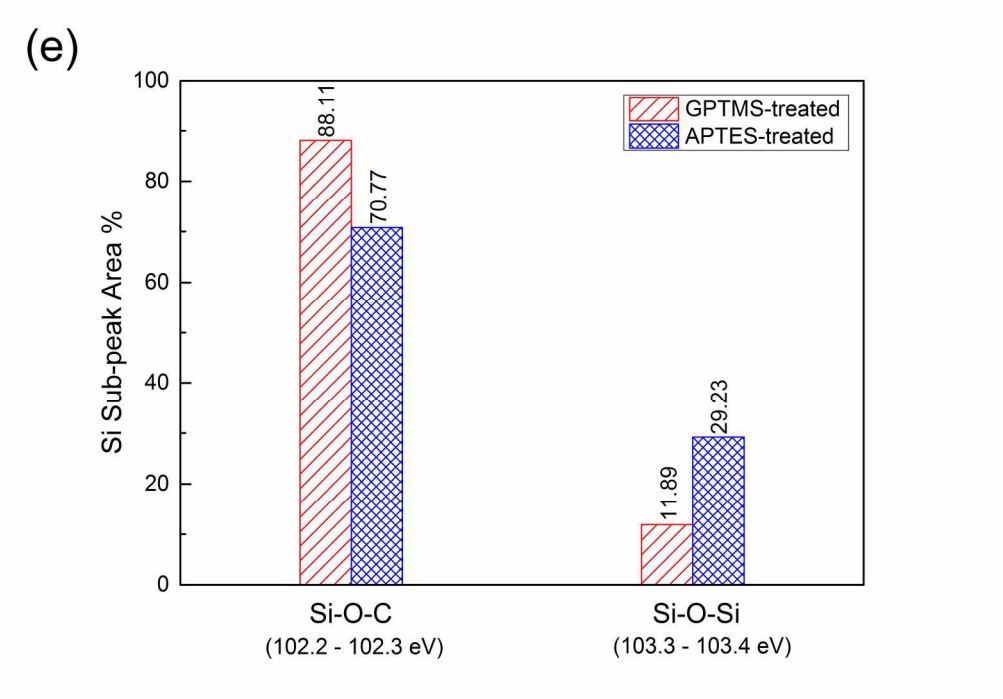

Figure 6. Comparison of different element binding types between pristine and treated asphaltene based on spectra deconvolution: (a) C 1s, (b) O 1s, (c) N 1s, (d) S 2p; and (e) Si 2p
201x141mm (300 x 300 DPI)

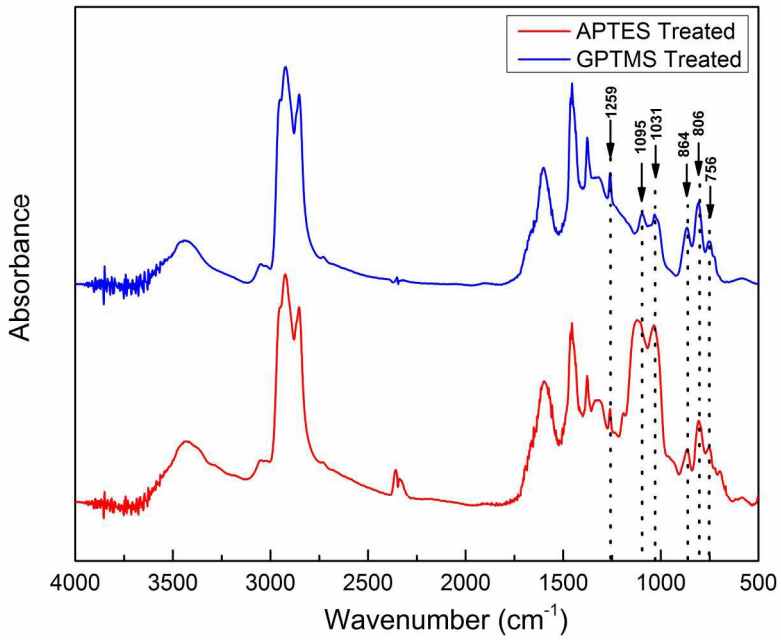

Figure 7. FTIR spectra of APTES- and GPTMS-treated asphaltene
215x166mm (300 x 300 DPI)

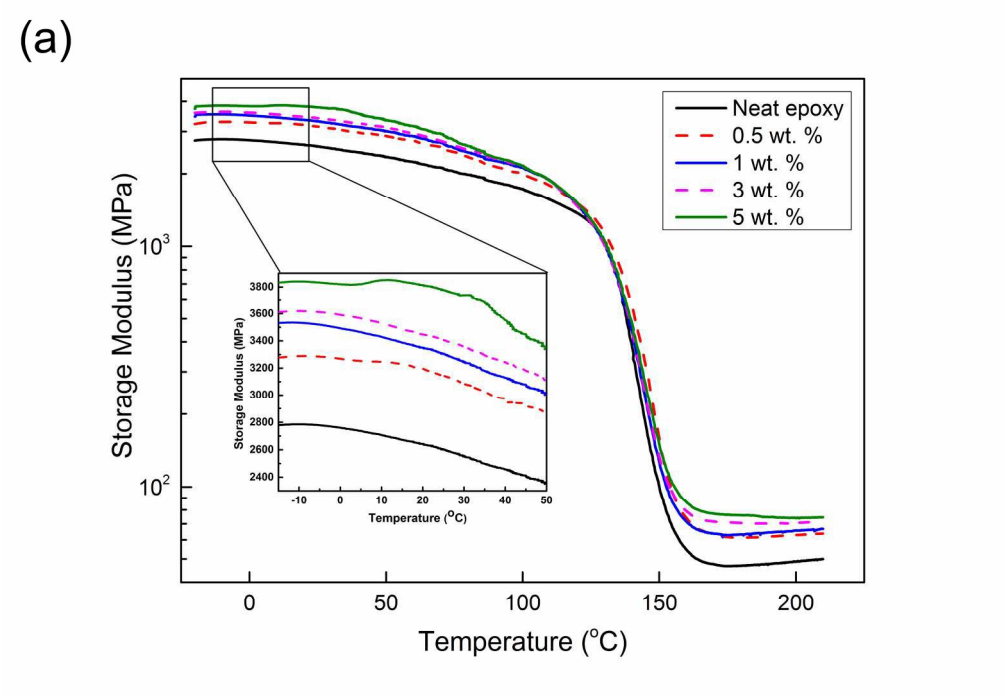

Figure 8. (a) Storage modulus (*E'*) and (b) *tan δ* of epoxy composites reinforced by GPTMS-treated asphaltene at different loading levels
201x141mm (300 x 300 DPI)

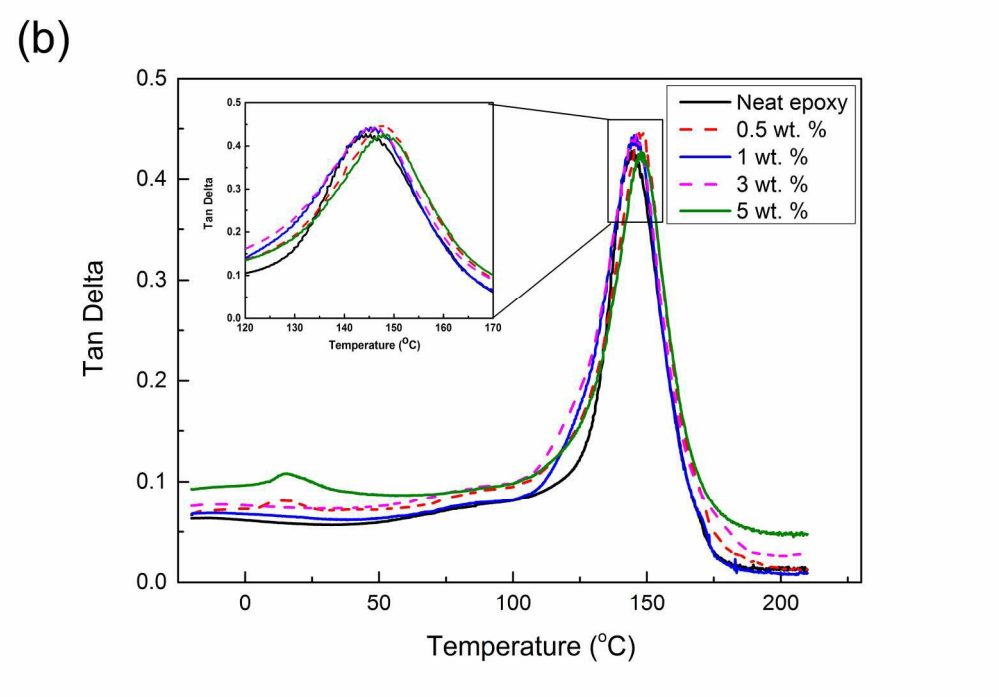

Figure 8. (a) Storage modulus (*E′*) and (b) *tan δ* of epoxy composites reinforced by GPTMS-treated asphaltene at different loading levels
201x141mm (300 x 300 DPI)

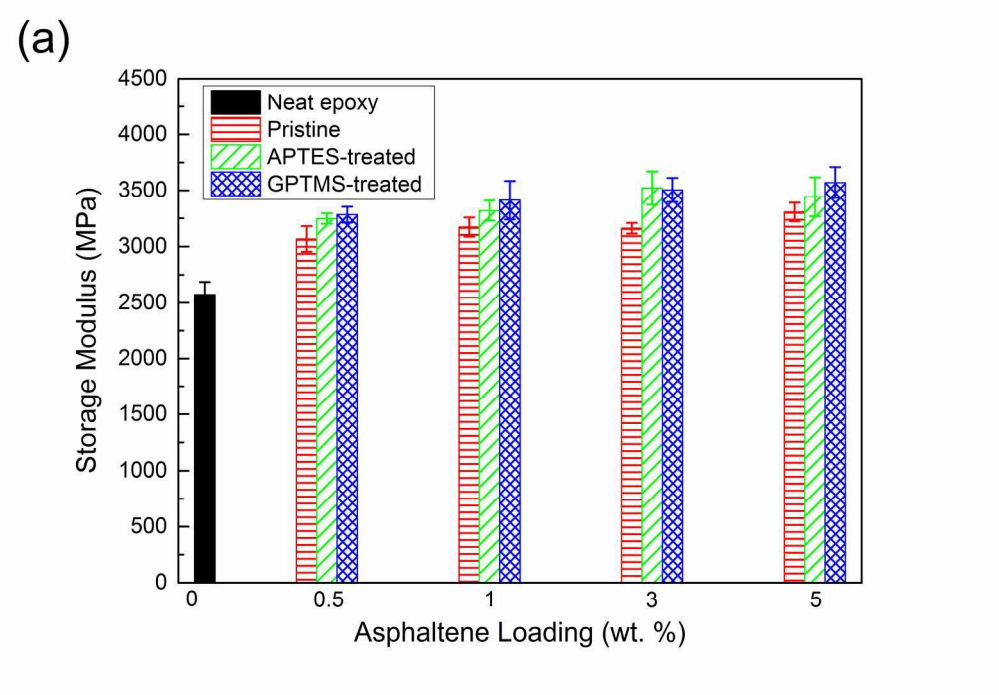

Figure 9. Comparison of (a) storage modulus (*E'*) at 25 °C and (b) T_g of asphaltene/epoxy composites
201x141mm (300 x 300 DPI)

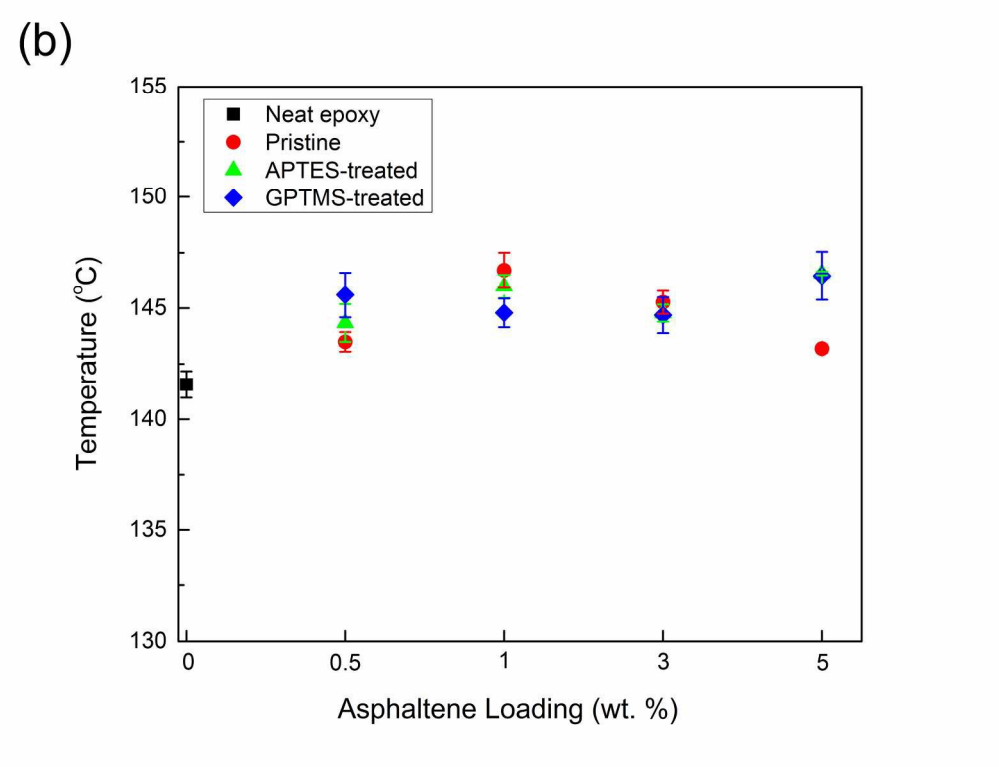

Figure 9. Comparison of (a) storage modulus (*E′*) at 25 °C and (b) T_g of asphaltene/epoxy composites
215x166mm (300 x 300 DPI)